Received: 18 January 2020 | Revised: 6 April 2020 | Accepted: 15 April 2020

DOI: 10.1002/wrna.1598

ADVANCED REVIEW

WIREs RNA WILEY

Unraveling the structure and biological functions of RNA triple helices

Jessica A. Brown

Department of Chemistry and Biochemistry, University of Notre Dame, Notre Dame, Indiana

Correspondence
Jessica A. Brown, Department of Chemistry and Biochemistry, University of Notre Dame, Notre Dame, IN 46556.
Email: jbrown33@nd.edu

Funding information
Henry Luce Foundation; National Institute of General Medical Sciences, Grant/Award Number: R35GM133696; University of Notre Dame

Abstract

It has been nearly 63 years since the first characterization of an RNA triple helix in vitro by Gary Felsenfeld, David Davies, and Alexander Rich. An RNA triple helix consists of three strands: A Watson–Crick RNA double helix whose major-groove establishes hydrogen bonds with the so-called "third strand". In the past 15 years, it has been recognized that these major-groove RNA triple helices, like single-stranded and double-stranded RNA, also mediate prominent biological roles inside cells. Thus far, these triple helices are known to mediate catalysis during telomere synthesis and RNA splicing, bind to ligands and ions so that metabolite-sensing riboswitches can regulate gene expression, and provide a clever strategy to protect the 3′ end of RNA from degradation. Because RNA triple helices play important roles in biology, there is a renewed interest in better understanding the fundamental properties of RNA triple helices and developing methods for their high-throughput discovery. This review provides an overview of the fundamental biochemical and structural properties of major-groove RNA triple helices, summarizes the structure and function of naturally occurring RNA triple helices, and describes prospective strategies to isolate RNA triple helices as a means to establish the "triplexome".

This article is categorized under:

RNA Structure and Dynamics > RNA Structure and Dynamics
RNA Structure and Dynamics > RNA Structure, Dynamics and Chemistry
RNA Structure and Dynamics > Influence of RNA Structure in Biological Systems

KEYWORDS

base triples, catalytic triplex, riboswitch, RNA stability element, RNA triple helix, telomerase, triplexome

1 | INTRODUCTION

Nucleic acids are largely thought to perform their biological functions as single- or double-stranded structures. In 1953, Watson and Crick reported the structure of DNA, whereby the nitrogenous bases of two anti-parallel DNA strands interact

via hydrogen bonds to form the canonical "Watson–Crick" base pairs: A-T and G-C (Watson & Crick, 1953). Similar interactions were later discovered for double-stranded RNA: The A-U and G-C Watson–Crick base pairs along with a non-canonical G•U Wobble base pair (in text, "-" denotes Watson–Crick base pair and "•" denotes Hoogsteen base pair or other non-Watson–Crick interactions; A. Rich & Watson, 1954; A. D. Rich & Davies, 1956; Varani & McClain, 2000). In 1957, Felsenfeld and co-workers deduced the formation of RNA triple helices in vitro by noting a minimum in absorbance when poly(U) and poly(A) RNAs were mixed together at a 2:1 ratio (Felsenfeld, Davies, & Rich, 1957). Subsequent characterization of these structures confirmed that the additional poly(U) strand binds along the major-groove of the poly(A-U) duplex, forming a major-groove triple helix of stacked U•A-U base triples (Arnott & Bond, 1973; Arnott, Bond, Selsing, & Smith, 1976; Hoogsteen, 1959). A U•A-U base triple is defined by multiple hydrogen bonds: A-U maintains canonical Watson–Crick base pairing with two hydrogen bonds and U•A forms a Hoogsteen base pair that involves two hydrogen bonds (Figure 1a), hence the third strand is commonly referred to as the Hoogsteen strand. Early on, studies focused on triple helices formed inside a test tube; therefore, one major outstanding question lingered: Do triple helices exist inside cells?

When Felsenfeld and co-workers first deduced the formation of a poly(U•A-U) triple helix, they posited that a naturally occurring triple helix could be comprised of double-stranded genomic DNA and single-stranded RNA (Felsenfeld et al., 1957). This biological scenario was eventually realized in the late 2000s when it was reported that noncoding RNAs, such as long noncoding RNAs (lncRNAs) and microRNAs (miRNAs), regulate gene expression via formation of RNA•DNA–DNA (R•D-D) triple helices, that is, RNA binds to major groove of genomic DNA (see [Li, Syed, & Sugiyama, 2016] for a review). However, the first direct observation of RNA base triples was in the X-ray crystal structure of $tRNA^{Phe}$ and the first direct observation of a poly(U•A-U)-derived triple helix was revealed in an NMR structure of human telomerase RNA, which has three consecutive U•A-U major-groove base triples (Table 1; Holbrook, Sussman, Warrant, & Kim, 1978; Sussman, Holbrook, Warrant, Church, & Kim, 1978; Theimer et al., 2005). Since then, it has been established that RNA triple helices can perform a variety of cellular functions: Metal-ion binding to facilitate

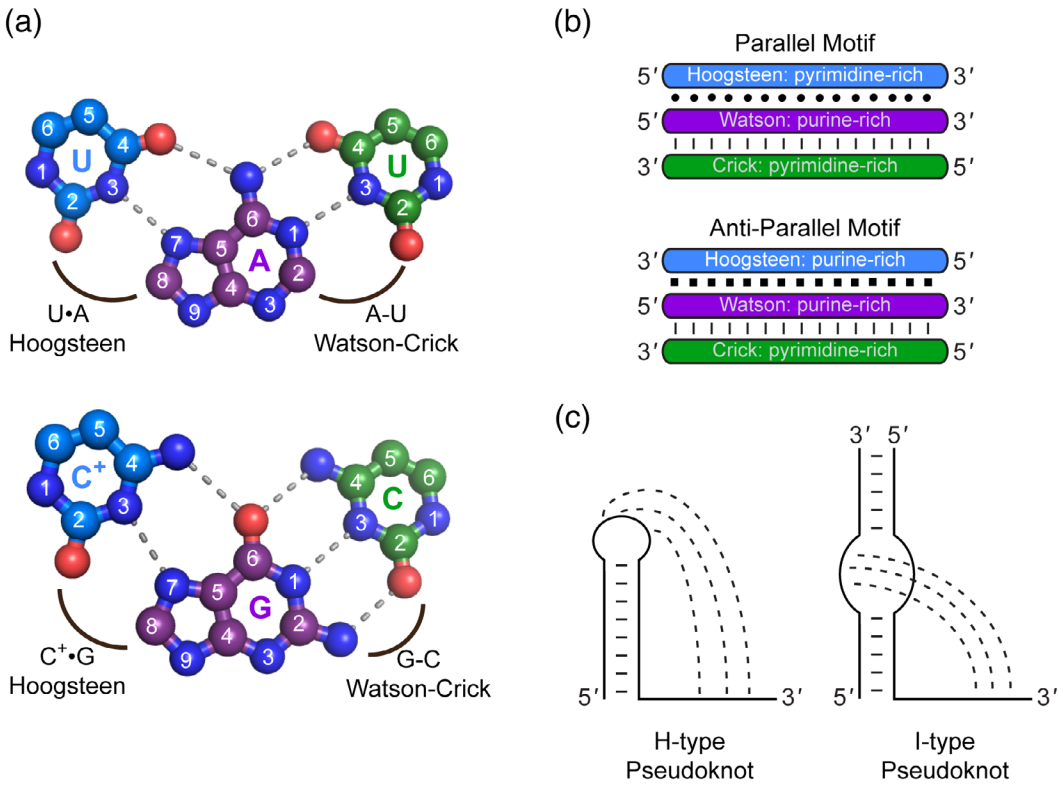

FIGURE 1 Composition and structural arrangement of major-groove RNA triple helices. Hydrogen-bonding interactions (gray dashed lines) are shown for the two canonical major-groove base triples: (a) U•A-U and C^+•G-C (ball-and-stick representation of base triples from PDB 6SVS; Ruszkowska, Ruszkowski, Hulewicz, Dauter, & Brown, 2020). Interactions are shown along with the Hoogsteen and Watson–Crick faces. (b) Schematics are shown for strand polarity and nucleotide composition in parallel and anti-parallel motifs. Interbase interactions are represented as a circle (•) for Hoogsteen base pair, a single dash (–) for Watson–Crick base pair, and a square (■) for reverse Hoogsteen base pair. (c) Major-groove RNA triple helices are commonly found in H-type or I-type pseudoknot structures. The three strands of triple helix are identified by the following tricolor scheme: Hoogsteen strand is blue, Watson strand is purple, and Crick strand is green

catalysis by self-splicing group II introns and the spliceosome, ligand binding by riboswitches that control gene expression, and protecting RNA from degradation (Conrad, 2014). Importantly, these RNA triple helices have been found in eukaryotic, prokaryotic, and viral RNAs, suggesting that they are widespread throughout nature. However, finding RNA tertiary interactions such as stacked base triples is an imposing challenge. Thus, developing experimental tools that can rapidly discover and validate triple helices with high accuracy is clearly needed. This review describes the fundamental biochemical and structural features of major-groove RNA triple helices, the structure and function of naturally occurring major-groove RNA triple helices, and then discusses methods that could be developed for the global discovery of RNA triple helices.

2 | FUNDAMENTAL PROPERTIES OF RNA TRIPLE HELICES

2.1 | Classification system of RNA triple helices

In nature, both major- and minor-groove triple helices have been observed. A minor-groove triple helix forms when the third strand interacts along the minor-groove edge, rather than major-groove, of an RNA duplex (see [Devi, Zhou, Zhong, Toh, & Chen, 2015; Lescoute & Westhof, 2006] for a review). The A-minor motif is a well-known minor-groove base triple and this tertiary interaction stabilizes large RNA structures, such as self-splicing introns and the ribosome as well as ribosomal frameshifting pseudoknots (Adams, Stahley, Kosek, Wang, & Strobel, 2004; Lescoute & Westhof, 2006; Nissen, Ippolito, Ban, Moore, & Steitz, 2001; Su, Chen, Egli, Berger, & Rich, 1999; Szewczak, Ortoleva-Donnelly, Ryder, Moncoeur, & Strobel, 1998; Toor et al., 2008). Naturally occurring major-groove RNA triple helices, such as telomerase RNA, are sometimes adjacent to a minor-groove triple helix or have intervening minor-groove base triples (Theimer et al., 2005). Importantly, minor-groove triple helices are usually not stable in isolation; therefore, this review will focus on major-groove RNA triple helices.

Major-groove triple helices are defined as parallel or anti-parallel. This nomenclature refers to the 5′–3′ polarity of the third strand with respect to the polypurine strand of the Watson–Crick duplex: A parallel orientation establishes Hoogsteen interactions whereas an anti-parallel orientation establishes reverse Hoogsteen interactions (Figure 1b). Triple helices can also be labeled as pyrimidine or purine motif, and this nomenclature reflects the predominant nucleobase in the third strand: The pyrimidine motif is U- or C-rich whereas the purine motif is A- or G-rich. In general, the pyrimidine motif favors a parallel orientation whereas the purine motif favors an anti-parallel orientation (Figure 1b). Within folded RNA structures, the pyrimidine motif is commonly found within H- or I-type pseudoknots (Figure 1c). Of note, there is experimental evidence that supports (Kalwa et al., 2016; Mondal et al., 2015; O'Leary et al., 2015; Zhao, Senturk, Song, & Grummt, 2018) and does not support (Escude et al., 1993; Morgan & Wells, 1968; Semerad & Maher 3rd., 1994) the formation of purine-motif triple helices when the third strand is RNA. Finally, RNA triple helices are defined by their molecularity: Intramolecular is where the three strands belong to the same transcript and intermolecular is where the three strands originate from two or three different transcripts. The primary focus of this review article will be intramolecular pyrimidine-motif RNA triple helices.

2.2 | Nucleotide composition of RNA triple helices

Pyrimidine-motif major-groove RNA triple helices are most commonly composed of the two canonical base triples: U•A-U and C^+•G-C (Figure 1a and Table 1). Unlike the U•A-U base triple, the C^+•G-C base triple is pH sensitive, for the pK_a at the N3 position of cytosine is ~4.6 (Levene, Bass, & Simms, 1926). For a Hoogsteen C^+•G base pair, protonation at the N3 position of cytidine establishes a hydrogen bond with N7 of guanosine so that two hydrogen bonds stabilize the Hoogsteen face, similar to U•A (Figure 1a). Thus, it is not surprising that C•G-C-containing triple helices are more stable at lower pH (i.e., ~5) compared to neutral pH (Brown, Valenstein, Yario, Tycowski, & Steitz, 2012; James, Brown, & Fox, 2003; Roberts & Crothers, 1996; Volker & Klump, 1994; S. Wang, Friedman, & Kool, 1995). Importantly, the pK_a of the Hoogsteen cytidine depends on its location within the triple helix and the identity of adjacent base triples. Most pK_a studies have examined DNA triple helices, although there are key conclusions that likely apply to RNA triple helices: (a) the pK_a of C•G-C base triples in DNA triple helices is usually >4, with observed pK_a values shifting as high as 9.5 and (b) the greatest pK_a shifts occur when the C•G-C base triple resides at an internal (not terminal) location within the triple helix, is flanked by T•A-T (not C•G-C) base triples, and the triple helix is intramolecular (not

TABLE 1 Summary of three-dimensional structures solved for natural RNAs containing a major-groove triple helix

RNA source	Base triples		Structure	Part of RNP?	References
	No.	Identity			
Telomerase					
Human TR	3	U•A-U	NMR (PDB 1YMO, 2K95, 2K96)	Yes, cryo-EM structure of holoenzyme (EMD-7521)	Kim et al. (2008), Nguyen et al. (2018), Theimer, Blois, and Feigon (2005)
Kluyveromyces lactis TR	1 5	C•G-C U•A-U	NMR (PDB 2M8K)	Yes, but no structure of holoenzyme	Cash et al. (2013)
Tetrahymena thermophila TER	2 1	U•A-U A•G-C	NMR (PDB 5KMZ)	Yes, cryo-EM structure of holoenzyme (EMD-6443)	Jiang et al. (2015)
Splicing					
Lactococcus lactis group IIA intron	1 1	G•G•U C•C-G	Cryo-EM (PDB 5G2Y)	Yes, cryo-EM structure with LtrA (PDB 5G2X)	Qu et al. (2016)
Pylaiella littoralis Group IIB intron	1 1 1	U•A-U G•G•U A•C-G	X-ray crystallography (PDB 6CHR)	Yes, but no structure with maturase	Chan et al. (2018)
Oceanobacillus iheyensis Group IIC intron	2 1	C•C-G G•G•U	X-ray crystallography (PDB 3BWP)[a]	Yes, but no structure with maturase	Toor, Keating, Taylor, and Pyle (2008)
Thermosynechococcus elongatus Group IIC intron	1 1 1	A•A-U G•G•U A•C-G	Cryo-EM (PDB 6MEC)	Yes, cryo-EM structure with maturase	Haack et al. (2019)
Human U2-U6 snRNAs	1 1 1	A•A-U G•G-C U•C-G	Cryo-EM (PDB 5MQF)[a]	Yes, cryo-EM structures of spliceosome	Bertram et al. (2017)
Saccharomyces cerevisiae U2-U6 snRNAs	1 1 1	A•A-U G•G-C U•C-G	Cryo-EM (PDB 5GMK)[a]	Yes, cryo-EM structures of spliceosome	Wan, Yan, Bai, Huang, and Shi (2016)
Schizosaccharomyces pombe U2-U6 snRNAs	1 1 1	A•A-U G•G-C U•C-G	Cryo-EM (PDB 3JB9)	Yes, cryo-EM structures of spliceosome	Hang, Wan, Yan, and Shi (2015), Yan et al. (2015)
Riboswitches					
Clostridium acetobutylicum c-di-GMP-II riboswitch	1 1 2 1	U•U-A G•G-C A•C-G c-di-GMP•A-U	X-ray crystallography (PDB 3Q3Z)	Unknown	Smith, Shanahan, Moore, Simon, and Strobel (2011)
Thermobifida fusca ykkC Guanidine-III riboswitch	1 1 2 1	GAI•(G•A-U•C) (A•C-G)•GAI G•G-C U•C-G	X-ray crystallography (PDB 5NWQ)	Unknown	L. Huang, Wang, Wilson, and Lilley (2017)
Lactobacillales rhamnosus $PreQ_1$-II riboswitch	1 2	A•U•$PreQ_1$•C U•A-U	X-ray crystallography (PDB 4JF2)	Unknown	Liberman, Salim, Krucinska, and Wedekind (2013)
Streptococcus pneumoniae $PreQ_1$-II riboswitch	1 2	A•U•$PreQ_1$•C U•A-U	NMR (PDB 2MIY)	Unknown	Kang, Eichhorn, and Feigon (2014)

TABLE 1 (Continued)

RNA source	Base triples		Structure	Part of RNP?	References
	No.	Identity			
Faecalibacterium prausnitzii $PreQ_1$-III riboswitch	1 2 1	A•U•$PreQ_1$•C U•A-U A•A-U	X-ray crystallography (PDB 4RZD)	Unknown	Liberman et al. (2015)
Sargasso Sea metagenome SAM-II riboswitch	1 1 1 1 2	A•A•U G•G-C A•C-G U•U•A_{SAM} U•A-U	X-ray crystallography (PDB 2QWY)	Unknown	Gilbert, Rambo, Van Tyne, and Batey (2008)
Candidatus Pelagibacter ubique HTCC1062 *met*Y SAM-V riboswitch	1 1 1 2 1	G•A-U A•G-C U•U•A_{SAM} U•A-U G•U•A	X-ray crystallography (PDB 6FZ0)	Unknown	L. Huang and Lilley (2018)
RNA stability elements					
Human MALAT1	9 1	U•A-U C•G-C	X-ray crystallography (PDB 4PLX)	Yes, but no structure with METTL16	Brown et al. (2014), Brown, Kinzig, DeGregorio, and Steitz (2016b), Warda et al. (2017)
Kaposi's sarcoma-associated herpesvirus PAN RNA	5	U•A-U	X-ray crystallography (PDB 3P22)	Unknown[b]	Mitton-Fry, DeGregorio, Wang, Steitz, and Steitz (2010)

Abbreviations: c-di-GMP, bis-(3′-5′)-cyclic dimeric guanosine monophosphate; GAI, guanidine; $PreQ_1$, 7-aminomethyl-7-deazaguanine (a precursor of the modified nucleoside, queuosine), and A_{SAM}, *S*-adenosylmethionine.
[a]Only a representative PDB ID is provided because there are too many to list. Refer to Galej, Toor, Newman, and Nagai (2018) for a more comprehensive list.
[b]None detected in the presence of HEK293 and HeLa cell lysate using an in vitro gel-shift assay (Brown et al., 2016b).

intermolecular; Asensio, Lane, Dhesi, Bergqvist, & Brown, 1998; Callahan, Trapane, Miller, Ts'o, & Kan, 1991; Leitner, Schroder, & Weisz, 2000; Plum & Breslauer, 1995; Singleton & Dervan, 1992; Xodo, Manzini, Quadrifoglio, van der Marel, & van Boom, 1991). These conclusions are generally thought to hold true considering two naturally occurring RNA triple helices, telomerase and human metastasis-associated lung adenocarcinoma transcript 1 (MALAT1), are destabilized inside cells (i.e., physiological pH) when their triple helices are mutated to have two or more consecutive C•G-C base triples (Brown et al., 2014; Brown, Kinzig, DeGregorio, & Steitz, 2016a; Shefer et al., 2007). Nonetheless, studying the pK_a shifts of C^+•G-C base triples in RNA triple helices is an area that requires more investigation.

As canonical base triples, U•A-U and C^+•G-C are the most stable major-groove base triples, although almost every possible base triple combination (N•N-N, where N = A, C, G or U) has been observed in three-dimensional RNA structures (Abu Almakarem, Petrov, Stombaugh, Zirbel, & Leontis, 2012; Firdaus-Raih, Harrison, Willett, & Artymiuk, 2011). A majority of these base triples were detected in rRNA from three-dimensional (3D) structures of the ribosome; therefore, these base triples are minor-groove base triples or they are isolated instances, meaning they are not stacked atop one another to form a major-groove triple helix. In the context of a U•A-U-rich major-groove RNA triple helix, systematic studies are gradually being conducted to better understand the stability of noncanonical RNA base triples, which is any base triple other than U•A-U or C^+•G-C. Here, the nucleotide composition of a single base triple is varied within a naturally occurring MALAT1 RNA triple helix (Brown et al., 2016a) or non-naturally occurring RNA triple helix (Kunkler et al., 2019). These studies employed native gel-shift assays and a cell-based intronless β-globin reporter assay to measure the relative stability of base triples. Despite the different RNA sequence and structural contexts, several notable themes emerged: The canonical U•A-U and C•G-C base triples are most stable, noncanonical base triples are most stable when a pyrimidine fills the Hoogsteen position (e.g., U•G-C, U•G-U, C•C-G, U•C-G), and four consecutive base triples of U•A-U, C•G-C, or U•G-C support the formation of a triple helix. Another study exchanged

nucleotide composition for the entire strand, rather than a single base triple, and found that poly(inosine•A-U), poly(inosine•inosine-C), and poly(G•G-C) form triple helices, although no natural counterparts have been identified to date (Letai, Palladino, Fromm, Rizzo, & Fresco, 1988). Interestingly, modified ribonucleotides expand the variety of base triples even further. Riboswitches engage modified nucleobases, ribonucleosides, and ribonucleotides of natural ligands in base triple formation to complete coaxial helical stacking (Table 1 and see Section 3.3 for details). With 143 modified ribonucleosides currently known (McCown et al., 2020), there is the potential for chemically diverse base triples to reside in yet-to-be-discovered naturally occurring RNA triple helices.

2.3 | Fine structural parameters of RNA triple helices

The structural parameters of DNA and RNA double helices have been rigorously established, with the earliest structural parameters being extrapolated from X-ray fiber diffraction data and eventually high-resolution X-ray crystal structures (Drew et al., 1981; Schindelin et al., 1995). For RNA triple helices, the structural parameters of poly(U•A-U) structures were derived from models generated using a combination of X-ray fiber diffraction data and computational modeling (Arnott & Bond, 1973; Arnott et al., 1976; Chandrasekaran, Giacometti, & Arnott, 2000; Raghunathan, Miles, & Sasisekharan, 1995). More recently, an X-ray crystal structure was solved for a U•A-U-rich RNA triple helix spanning 11 consecutive base triples, thereby revealing the global and local structural parameters (Figure 2 and Table 2; Ruszkowska et al., 2020). Overall, the right-handed RNA triple helix, which has a central C•G-C base triple flanked on both sides by five U•A-U base triples, is an A-family conformer and is quantitatively similar to A′-RNA, which is effectively an underwound form of A-RNA (Table 2; Arnott, Hukins, Dover, Fuller, & Hodgson, 1973; Ruszkowska et al., 2020; Tanaka et al., 1999). Despite the presence of a Hoogsteen strand, the RNA triple helix has a diameter of 24 Å, which is nearly identical to those of double helices (Table 2). Similar to the values determined from X-ray fiber diffraction-based models of poly(U•A-U) triple helices, the helical pitch (i.e., height of a full turn) is relatively tall at 35.1 Å with adjacent base triples spaced 2.9 Å apart vertically and rotated about the helical axis at a ~30° twist (Table 2; Arnott & Bond, 1973; Arnott et al., 1976). Therefore, one complete helical turn contains 12 base triples, which is greater than the number of base pairs per turn in both A-RNA and B-DNA (Table 2). This helical unwinding accommodates the Hoogsteen strand. Here, the major-groove width increases from 3.1 Å in A-RNA to 9.2 Å for the double helix of the RNA triple helix (Figure 2 and Table 2). This expansion of the major groove is made possible by a reduced inclination angle (i.e., tilt of base pair with respect to helical axis) to 8.4°, thereby allowing the Hoogsteen strand to occupy nearly all the major groove (i.e., major-groove width is only 2.3 Å between Hoogsteen and Crick strands; Figure 2 and Table 2). Importantly, this structure of a U•A-U-rich RNA triple helix definitively shows that all three strands have glycosidic bonds in the *anti*-conformation and riboses that favor the C3′-*endo* sugar pucker conformation, which is consistent with structures solved for naturally occurring RNA triple helices. Future studies are needed to determine how the fine structural parameters for this U•A-U-rich RNA triple helix compare to those of other triple helices, particularly a C^+•G-C-rich RNA triple helix or a T•A-T-rich DNA triple helix. Altogether, understanding the fundamental biochemical and structural principles of RNA triple helices provides insights into the structural makeup that would be possible for naturally occurring RNA triple helices.

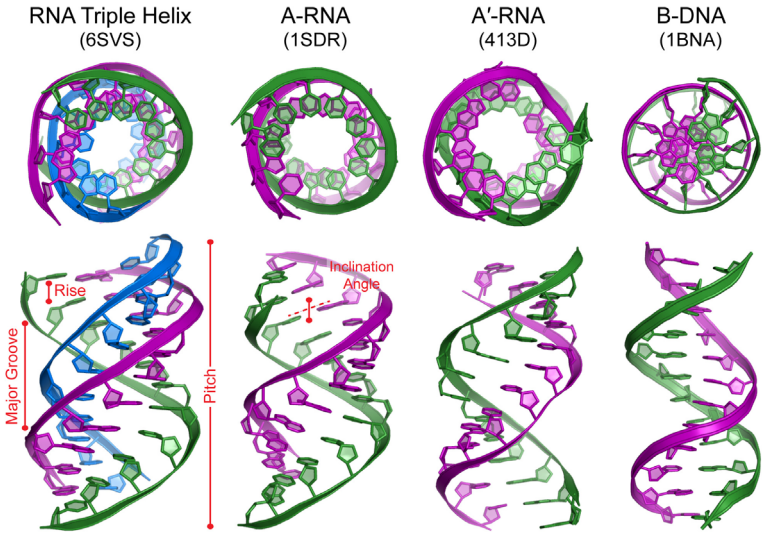

FIGURE 2 Structural views of triple and double helices. The top and side views are shown for X-ray crystal structures (cartoon representation) solved for an RNA triple helix, A-RNA double helix, A′-RNA double helix, and B-DNA double helix. Hoogsteen strand is blue, Watson (or purine-rich) strand is purple, and Crick (or pyrimidine-rich) strand is green. Select structural parameters are defined by red text and pictures. The PDB IDs for displayed structures are listed below each name

TABLE 2 Computed values of various structural parameters

Parameter	RNA triple helix[a]	A-RNA double helix	A′-RNA double helix	B-DNA double helix
Helical sense	Right handed	Right handed	Right handed	Right handed
Diameter (Å)	24	22.9	24	23.9
Helix pitch (Å)	35.1	27.5	32.8	33.7
Helical rise per base pair or base triple (Å)	2.9	2.6	2.9	3.4
Helical twist (°)	29.7	33.7	31.4	36.2
Base pairs per helical turn or base triples per helical turn	12	10.7	11.5	10
Axial displacement (Å)	−5.0	−3.9	−4.9	0.3
Major-groove dimensions				
Width (Å)	9.2 (2.3)	3.1	8.4	11.4
Depth (Å)	11.0	9.2	9.3	4.5
Minor-groove dimensions				
Width (Å)	9.0	9.9	9.7	4.9
Depth (Å)	1.5	0.5	0.5	5.3
Inclination angle (°)	8.4	17.6	13.6	−0.5
Glycosidic bond conformation	*Anti*	*Anti*	*Anti*	*Anti*
Sugar pucker conformation	C3′ *endo*	C3′ *endo*	C3′ *endo*	C2′ *endo*

Note: Values obtained from Ruszkowska et al. (2020).
[a]All values computed using only the double helix portion of RNA triple helix except for parenthetical 2.3, which is major-groove width between Hoogsteen and Crick strands.

3 | STRUCTURE AND FUNCTION OF NATURAL RNA TRIPLE HELICES

Experimental techniques to detect major-groove triple helices in nucleic acids include circular dichroism spectroscopy, oligonucleotide binding assays (e.g., isothermal titration calorimetry, native gel-shift assay, surface plasmon resonance), fluorescence resonance energy transfer, infrared spectroscopy, structure mapping (chemical or nuclease), UV thermal denaturation assay, and compensatory base triple mutations (e.g., stepwise substitution of putative U•A-U with C^+•G-C base triple) coupled with functional assay appropriate for triple helix-of-interest. These techniques generate results that would be consistent with the formation of a triple helix. Importantly, direct evidence comes from solving 3D structures using X-ray crystallography, nuclear magnetic resonance (NMR), or single-particle cryogenic-electron microscopy (cryo-EM) methodologies. Because simplified in vitro systems for structural studies can artificially induce the formation of a triple helix, it is ideal to have a cell-based assay in which the parent RNA harboring the triple helix, either endogenous or exogenous, can be studied in its true physiological environment. To validate an RNA triple helix, experimental evidence from two or more orthogonal approaches is desired, preferably direct evidence coupled with a cell-based assay examining compensatory base triple mutants. The structure and function of natural RNA triple helices, defined herein as two consecutive base triples along helical axis, that have been visualized using X-ray crystallography, NMR and/or cryo-EM are described below. Thus far, three major biological functions have been determined: Catalysis, ligand binding, and stability element.

3.1 | RNA triple helix is required for telomerase catalytic activity

Telomerase is the ribonucleoprotein (RNP) complex responsible for synthesizing telomeres, which are structures that protect the ends of linear chromosomes (see [Wu, Upton, Vogan, & Collins, 2017] for review). The minimal telomerase RNP consists of telomerase RNA (TR, also known as hTR, TERC, TER in ciliates or TLC1 in yeast), a noncoding RNA which provides a template for the synthesis of telomeres (Greider & Blackburn, 1989), and telomerase reverse transcriptase (TERT), which possesses de novo nucleotidyl transferase activity to synthesize telomeric DNA repeats (Lingner

et al., 1997; Nakamura et al., 1997). Although TRs are divergent in size (~150 to >3,000 nucleotides) and sequence, their structures from various eukaryotic organisms, such as budding yeast, ciliates, and vertebrates, have a conserved H-type pseudoknot (Figures 1c and 3) that includes a major-groove triple helix (Cash et al., 2013; J. L. Chen, Blasco, & Greider, 2000; Shefer et al., 2007; Theimer et al., 2005; Tzfati, Knight, Roy, & Blackburn, 2003; Ulyanov, Shefer, James, & Tzfati, 2007).

Human TR was the first naturally occurring U•A-U major-groove RNA triple helix to have its 3D structure solved, which was almost 50 years after poly(U•A-U) triple helices had been reconstituted in a test tube by Felsenfeld and co-workers (Felsenfeld et al., 1957; Theimer et al., 2005). Since then, solution NMR structures have been solved for human TR (Figure 3), *Kluyveromyces lactis* TR and *Tetrahymena thermophila* TER (Table 1; Cash et al., 2013; Cash & Feigon, 2017; Kim et al., 2008; Theimer et al., 2005). These structures show that the major-groove triple helix is composed of two to five U•A-U base triples along with a protonated C^+•G-C base triple in *K. lactis* and a protonated A^+•G-C base triple in *T. thermophila* (Table 1; Cash et al., 2013; Cash & Feigon, 2017; Kim et al., 2008; Theimer et al., 2005). These major-groove triple helices are extended by nearby minor-groove base triples, forming a nearly continuous triple helix that may form cooperatively (Cash & Feigon, 2017; Chen, Chang, Chou, Bustamante, & Tinoco Jr., 2009; Kim et al., 2008; Theimer et al., 2005). Importantly, the presence of a major-groove triple helix in TR is further supported by mutating individual U•A-U base triples to the isosteric C•G-C base triple (Cash et al., 2013; Cash & Feigon, 2017; G. Chen et al., 2009; Qiao & Cech, 2008; Shefer et al., 2007; Theimer et al., 2005). For human TR, this compensatory mutational analysis showed that the C•G-C-containing mutant is thermodynamically more stable at pH 5 than pH 7 based on UV thermal denaturation assays and that the complete triple mutation is necessary to recover telomerase activity in an in vitro TRAP (telomeric repeat amplification protocol) assay, demonstrating that the triple helix is essential for catalysis (Theimer et al., 2005). A similar base triple compensatory mutational analysis was performed and similar outcomes were observed for *K. lactis*, *Saccharomyces cerevisiae* (TLC1) and *T. thermophila* TRs using various in vitro and cell-based assays to monitor telomerase activity (Cash et al., 2013; Cash & Feigon, 2017; Qiao & Cech, 2008; Shefer et al., 2007). Collectively, these studies demonstrate that the triple helix structure, not sequence, is conserved and is required for telomerase activity.

Originally, it was thought that the 2′-hydroxyl of A176, which participates in a U•A-U base triple, played a direct role in catalysis (Qiao & Cech, 2008). However, cryo-EM structures of the human and *Tetrahymena* telomerase holoenzyme both show the pseudoknot forming an arc-like structure that partially encircles TERT, positioning the triple helix on the opposite side of TERT's active site (Jiang et al., 2015; Nguyen et al., 2018). In light of these recent structural findings, it appears that the triple helix contributes to the proper folding of the pseudoknot, whose structure is essential for a fully assembled and catalytically active RNP (Cash et al., 2013; Cash & Feigon, 2017; Liu & Theimer, 2012; Mihalusova, Wu, & Zhuang, 2011; Qiao & Cech, 2008; Shefer et al., 2007; Theimer et al., 2005; Tzfati et al., 2003). Thus, the dynamics of a distal tertiary structural element are coupled to catalysis.

Although the pseudoknot is required for a fully active RNP, the triple helix is not required for *S. cerevisiae* TERT (Est2) to bind to TR (Qiao & Cech, 2008). Unfortunately, the low resolution of the telomerase holoenzyme cryo-EM structures prevents an in-depth analysis of how TERT directly interacts with the triple helix. It should also be

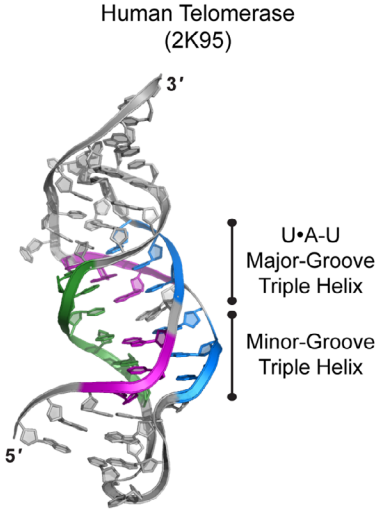

FIGURE 3 Triple helix in telomerase RNA. Telomerase RNA forms a nearly continuous triple helix (tricolor cartoon representation) in which a U•A-U major-groove triple helix is adjacent to a minor-groove triple helix

mentioned that a C•G-C major-groove base triple and a minor-groove C•U-A base triple stack atop each other in the CR4/5 domain of Japanese medaka telomerase TR (J. Huang et al., 2014). Neither of these base triples makes direct contacts with the telomerase RNA-binding domain of TERT (J. Huang et al., 2014). Additionally, an extended form of human TR transcripts (hTR exL) is predicted to form a triple helix that may recruit dyskerin or another protein (Tseng, Wang, Schroeder, & Baumann, 2018). Thus far, the structures of telomerase RNPs have not yielded any insights into how proteins interact with the various triple helices of TR. Because most TR pseudoknots have U•A-U base triples and A176 contributes to catalysis, it will be informative to learn how TERT directly recognizes, if at all, the major-groove triple helix of TR. Furthermore, telomerase has emerged as an attractive and novel target in cancer therapeutics because telomerase reactivation promotes human cell immortality and cancer, whereby telomerase activity is upregulated in >75% of tumor samples collected from multiple cancer types (Shay, 2016; Shay & Bacchetti, 1997). Therefore, a better understanding of the telomerase triple helix may enable the design of a novel therapeutic.

3.2 | RNA triple helix coordinates catalytic magnesium ions during splicing

Introns are intervening noncoding RNA sequences that are removed from precursor RNAs (e.g., mRNA, rRNA, and tRNA) in a process known as splicing. RNA splicing proceeds in two sequential phosphotransesterification reactions: First 5′ splice site cleavage and then 3′ splice site cleavage so that the two RNA segments can be ligated together. Interestingly, this splicing reaction occurs at a single catalytic center and requires a "catalytic triplex" for both group II introns and the eukaryotic spliceosome. High-resolution 3D structural studies of group II introns and the spliceosome have shown that their active site architectures are highly conserved, supporting the hypothesis that these RNA catalysts share a common molecular ancestor (see [Galej et al. (2018)] for review).

Group II introns are self-splicing ribozymes found in all three domains of life. Based on RNA secondary structures, group II introns are classified as IIA to IIF and are generally 400–800 nucleotides in length (see [Smathers and Robart (2019)] for a review). Group II introns form a six-domain structure (I–VI), with the catalytic triplex residing in domain V. A fully formed catalytic triplex consists of three consecutive base triples, which includes the so-called "catalytic triad" (Table 1; Chan et al., 2018; Haack et al., 2019; Marcia & Pyle, 2012; Toor et al., 2008). The catalytic triad is the most highly conserved region across group IIA–C introns. Two common catalytic triads are AGC and CGC, which refer to the nucleotides in the purine-rich strand of the catalytic triplex. For example, the AGC catalytic triad from the *Pylaiella littoralis* group IIB intron corresponds to the U•A-U/G•G-U/A•C-G catalytic triplex, where the underlined nucleotides denote the catalytic triad (Table 1; Chan et al., 2018). A combination of mutational, phosphorothioate substitution, and metal rescue analyses have shown that the catalytic triplex of the ai5γ group II intron from *S. cerevisiae* is essential for splicing because the phosphate backbone interacts with at least two divalent magnesium ions (Boulanger et al., 1995; Gordon, Fong, & Piccirilli, 2007; Gordon & Piccirilli, 2001; Sontheimer, Gordon, & Piccirilli, 1999). These two metal ions activate the nucleophile in the second step of splicing (i.e., exon-ligation) and stabilize the leaving groups during both splicing steps (Gordon et al., 2007; Gordon & Piccirilli, 2001; Sontheimer et al., 1999). 3D structural studies have subsequently confirmed that the negatively charged phosphate backbones of the catalytic triplex coordinate two magnesium ions with high affinity, consistent with a two metal-ion mechanism (Figure 4a; Chan et al., 2018; Haack et al., 2019; Marcia & Pyle, 2012, 2014; Robart, Chan, Peters, Rajashankar, & Toor, 2014; Steitz & Steitz, 1993; Toor et al., 2008). Along with metal binding, the triple helix is thought to mediate the transition between the two steps of splicing, for RNA structural probing studies and comparative analyses of crystallographic structures during the splicing reaction cycle have observed the catalytic triplex undergoing dynamic conformational transitions (Chan et al., 2018; Marcia & Pyle, 2012). Although group II introns require a maturase protein for activity in vivo, it appears that the maturase protein does not interact with the catalytic triplex, for the maturase protein is more than 10 Å from the catalytic triplex in a cryo-EM structure of the *Lactococcus lactis* group IIA intron-LtrA maturase complex (Qu et al., 2016). Altogether, most structural and mechanistic observations for the group II intron, including the catalytic triplex, apply to the eukaryotic spliceosome.

The eukaryotic spliceosome is an RNP complex whose composition is dynamic throughout the splicing cycle: Five small nuclear RNPs (i.e., U1, U2, U4, U5, and U6 snRNPs) and numerous proteins to form a multi-megadalton complex. This RNP is responsible for pre-mRNA splicing in eukaryotes (see [Wilkinson, Charenton, & Nagai, 2019] for review). Like group II introns, the active site of the spliceosome has a catalytic triplex that (a) includes a catalytic triad and (b) uses its phosphate backbone to coordinate two catalytic magnesium ions, which stabilize the leaving groups of each step in the splicing reaction (Figure 4a and Table 1; Fica, Mefford, Piccirilli, & Staley, 2014; Fica et al., 2013;

Gordon, Sontheimer, & Piccirilli, 2000; Sontheimer, Sun, & Piccirilli, 1997; Yean, Wuenschell, Termini, & Lin, 2000). The intermolecular catalytic triplex forms via Watson–Crick base pairing between the U2 and U6 snRNAs, and the Hoogsteen strand nucleotides in U6 snRNA includes two nucleotides (underlined GA) from the ACAGAGA sequence that recognizes the 5′-splice site of intron (Bertram et al., 2017; Fica et al., 2014; Hang et al., 2015; Mefford & Staley, 2009; Wan et al., 2016; Yan et al., 2015; Yan, Wan, Bai, Huang, & Shi, 2016). These interactions bring together the 5′-splice site and the metal-bound catalytic triplex at the active site. Thus far, cryo-EM structures of the spliceosome have predicted a relatively rigid catalytic center, including the catalytic triplex, once the activated spliceosome forms (L. Zhang, Vielle, Espinosa, & Zhao, 2019). In contrast, yeast genetic studies suggest the catalytic core undergoes conformational rearrangements, toggling between catalytically active and inactive conformations (Eysmont, Matylla-Kulinska, Jaskulska, Magnus, & Konarska, 2019). Most nucleobases in the U2–U6 catalytic triplex appear to be dispensable for splicing in *S. cerevisiae* whole-cell extract, suggesting that proteins play an important role in stabilizing the U2–U6 snRNAs (Bao, Boon, Will, Hartmuth, & Luhrmann, 2018). Unlike group II introns, the catalytic triplex of the spliceosome is embedded in a protein cavity; therefore, most RNA–protein contacts are established between the sugar-phosphate backbone of the catalytic triplex and the side chains of arginine, lysine, glutamine, and serine. However, a cryo-EM structure of the *S. cerevisiae* spliceosome C complex suggests that the side chain of His5 from CWC2P has the potential to mediate two hydrogen bonds: One with N2 of the Hoogsteen G in the G•G-C base triple and one with O6 of G in the U•C-G base triple (Figure 4b and Table 1; Wan et al., 2016). This putative arrangement illustrates a novel way in which proteins may recognize two stacked base triples. Finally, it should be mentioned that the minor spliceosome is predicted to form a similar catalytic triplex by the U6atac and U12 snRNAs based on sequence conservation and biochemical studies. The catalytic triplex in group II self-splicing introns and the spliceosome demonstrates how triple helices can mediate essential biological functions and likely more examples remain to be discovered.

3.3 | RNA triple helix as a ligand-binding site

Riboswitches are highly conserved RNA structural elements (or aptamers) used primarily by bacteria to control gene expression in response to intracellular ligand binding. As a *cis*-regulatory element typically in the 5′ untranslated region of mRNAs, riboswitches can sense ligands, usually a metabolite or ion, and subsequently adopt a ligand-bound structure that will accordingly turn transcription or translation ON/OFF (see [Breaker, 2018] for a review). Over 100,000 riboswitches have been discovered among ~47 riboswitch classes, which are classified by ligand identity (P. J. McCown, Corbino, Stav, Sherlock & Breaker, 2017).

Thus far, 3D structures have been solved for ~30 different riboswitch classes and six of them revealed a major-groove triple helix in their ligand-bound states: Cyclic-dimeric-guanosine monophosphate (c-di-GMP)-II, guanidine-III, prequeosine ($PreQ_1$)-II, $PreQ_1$-III, *S*-adenosylmethionine (SAM)-II, and SAM-V (Table 1; Gilbert et al., 2008; L. Huang & Lilley, 2018; L. Huang et al., 2017; Kang et al., 2014; Liberman et al., 2013; Liberman et al., 2015; Smith et al., 2011). In general, riboswitch triple helices are composed of two canonical U•A-U base triples and one to four noncanonical base triples that are arranged together in a classic H-type pseudoknot or a related variant (Figures 1c and 5). Importantly, the ligand in all six riboswitches is recognized by the triple helix. For the five RNA-derived ligands, their nucleobases participate in a noncanonical base triple or quadruplet (Figure 5 and Table 1). For example, the adenine moiety of SAM

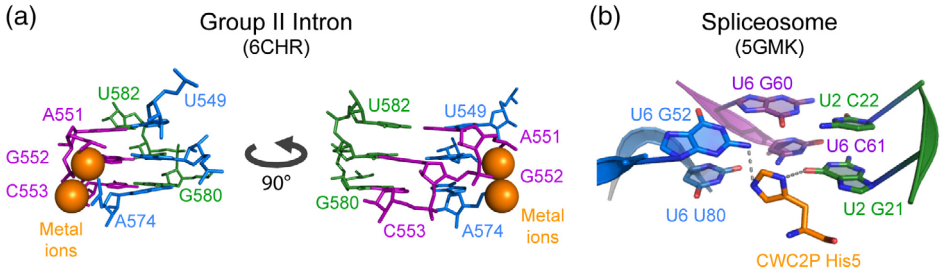

FIGURE 4 Catalytic triplexes involved in splicing. (a) The catalytic triplex of both the group II self-splicing intron (tricolor stick representation) and the spliceosome (not shown) coordinate two catalytic metal ions (orange spheres) via electrostatic interactions with phosphate backbone. Two views are shown. (b) His5 of CWC2P (orange stick representation) may form hydrogen bonds (gray dashed lines) with two of the three base triples (tricolor sticks) in the catalytic triplex observed for the *S. cerevisiae* spliceosome

is engaged in an A_{SAM}•U reverse Hoogsteen base pair of an A_{SAM}•U•U triple and $PreQ_1$ is recognized by cytidine via *trans*-Watson–Crick interactions in an A•U•$PreQ_1$•C quadruplet (Figure 5a,b; Gilbert et al., 2008; L. Huang & Lilley, 2018; Kang et al., 2014; Liberman et al., 2013; Liberman et al., 2015). In the c-di-GMP-II riboswitch crystal structure, the two guanine bases of c-di-GMP are differentially recognized: One guanine engages in a minor-groove c-di-GMP•A-U base triple whereas the other guanine forms hydrogen bonds with nearby nucleotides and a hydrated magnesium ion (Figure 5c; Smith et al., 2011). Interestingly, ligands that lack a nucleobase moiety can also be recognized by a triple helix. The one lone example, the guanidinium ion, is coordinated by a guanine in a noncanonical A•C-G base triple and another guanine in a G•A-U•C quadruplet (Figure 5d; L. Huang et al., 2017). Because several hundred "undiscovered" riboswitch classes are predicted (P. J. McCown, Corbino, Stav, Sherlock, & Breaker, 2017), it will be interesting to learn if these riboswitches use triple helices to capture ligands, particularly ligands that do not have chemical moieties mimicking nucleotides.

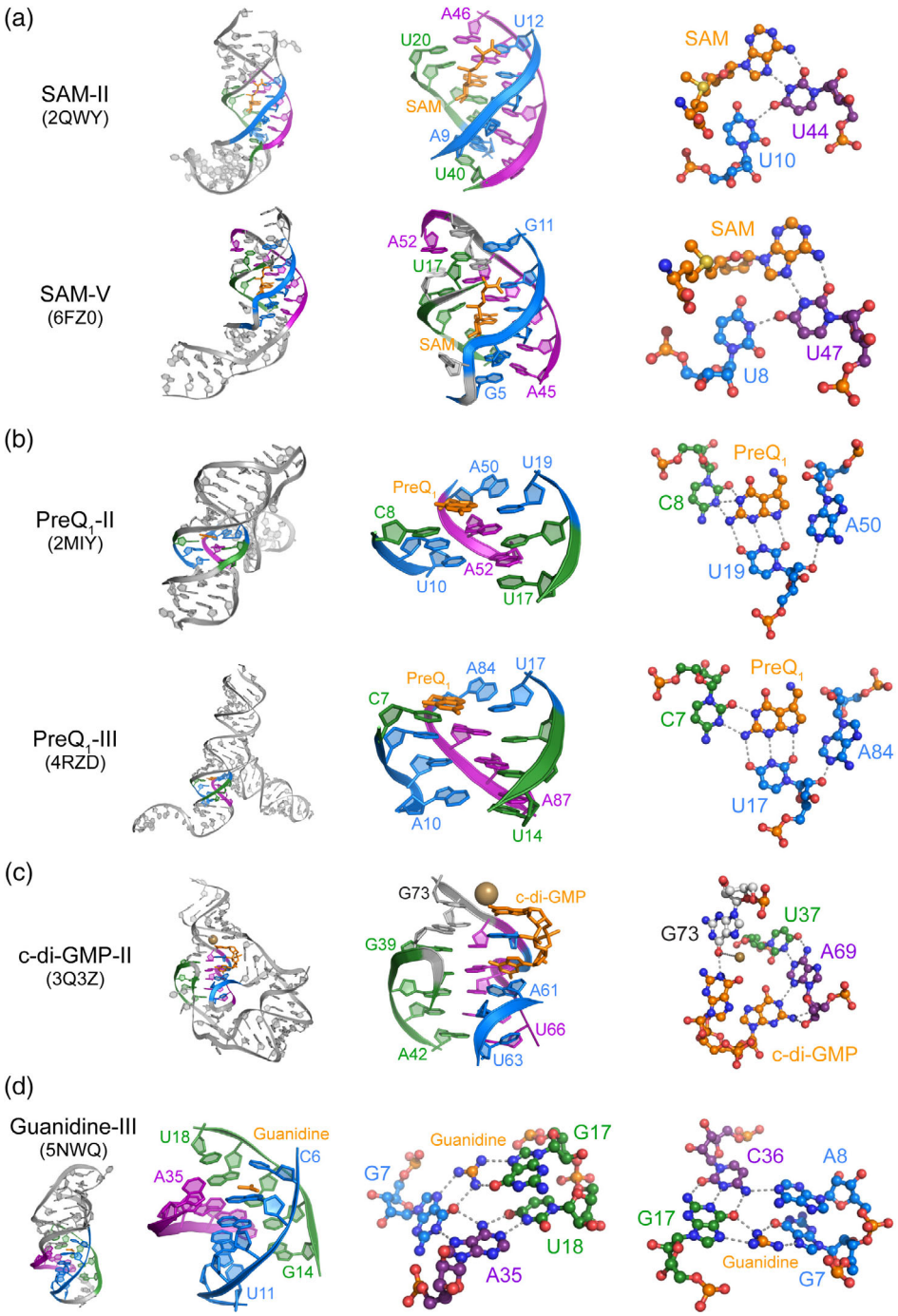

FIGURE 5 Structural basis of ligand recognition by an RNA triple helix. The 3D structures are shown for six ligand-bound riboswitches: (a) SAM-II, SAM-V, (b) $PreQ_1$-II, $PreQ_1$-III, (c) c-di-GMP-II, and (d) guanidine-III. For each riboswitch, there is a panel that displays the entire experimentally determined structure with PDB in parenthesis (left panel, cartoon representation), the triple helix interacting with ligand (middle panel, cartoon representation), and noncovalent interactions of ligand and nucleotides (right panel, ball-and-stick representation). The ligand is shown in orange and triple helix components are shown in tricolor scheme

With various binding modes of ligands and base triples being observed, it is not surprising that a broad range of equilibrium dissociation constants have been measured for the six riboswitch-ligand complexes: 200 pM to 2 nM for c-di-GMP-II, 60 μM for guanidine-III, 17.9 nM–6.6 μM for $PreQ_1$-II, 6.5–900 nM for $PreQ_1$-III, 670 nM for SAM-II, and 0.5–150 μM for SAM-V (Gilbert et al., 2008; L. Huang & Lilley, 2018; Kang et al., 2014; Lee, Baker, Weinberg, Sudarsan, & Breaker, 2010; Liberman et al., 2013; Liberman et al., 2015; P. J. McCown, Liang, Weinberg, & Breaker, 2014; Meyer, Roth, Chervin, Garcia, & Breaker, 2008; Poiata, Meyer, Ames, & Breaker, 2009; Sherlock & Breaker, 2017). Importantly, divalent ions can strengthen ligand-binding affinity up to 85-fold for the *Streptococcus pneumoniae* $PreQ_1$-II riboswitch (Kang et al., 2014), a finding that prompts the question: To what extent is the triple helix (or pseudoknot) formed in the absence of ligand (see [Jones & Ferre-D'Amare, 2017] for review on ligand-binding pocket conformations)? Having three electronegative strands, triple helices are more stable in the presence of magnesium ions (Felsenfeld et al., 1957). Thus, it is difficult to parse whether ligands bind to a preformed triple helix or if ligand binding induces the formation of a triple helix. At least for the *metX* SAM-II riboswitch, both magnesium and ligand-binding seem to be required for the fully-folded ligand-bound conformation, although magnesium plays a critical role in pre-organizing the riboswitch toward a binding-competent state but it still lacks the triple helix in the absence of SAM (B. Chen, Zuo, Wang, & Dayie, 2012; Haller, Rieder, Aigner, Blanchard, & Micura, 2011; Roy et al., 2017). Similarly, two U•A-U base triples in the *Lactobacillus rhamnosus* $PreQ_1$-II riboswitch include A nucleotides from the ribosome-binding site; therefore, the triple helix forms after ligand binding (Aytenfisu, Liberman, Wedekind, & Mathews, 2015; Liberman et al., 2013; Souliere et al., 2013; Warnasooriya et al., 2019). Another consideration is that proteins could participate in the folding and conformational states of some riboswitches, although proteins are not required for ligand binding to the current experimentally validated riboswitches (Breaker, 2012). Importantly, the RNA triple helix can mediate both ligand binding and expression output for select riboswitches and the functional coupling is only beginning to be understood (Dutta & Wedekind, 2019).

Finally, it should be noted that riboswitches using a triple helix as a ligand-binding site are not coupled to a single mechanism for controlling gene expression. The ligand-bound forms of the c-di-GMP-II (Lee et al., 2010) and guanidine-III (Sherlock & Breaker, 2017) riboswitches turn ON translation while $PreQ_1$-II (Dutta, Belashov, & Wedekind, 2018; Meyer et al., 2008; Neuner, Frener, Lusser, & Micura, 2018; Van Vlack, Topp, & Seeliger, 2017), $PreQ_1$-III (Liberman et al., 2015; Van Vlack et al., 2017), *metX* SAM-II (Gilbert et al., 2008), and SAM-V riboswitches (L. Huang & Lilley, 2018; Poiata et al., 2009) turn OFF translation. Thus, there are instances where ligand binding leads to sequestration of the ribosome-binding site into a triple helix to turn OFF translation and other instances where the ribosome-binding site is released upon ligand binding, thereby turning ON translation. Proteins are involved in these processes to turn translation ON/OFF. Ribosomal protein S1 interacts with various conformations of the *Thermoanaerobacter tengcongensis* $PreQ_1$-I riboswitch, a structure whose ligand-binding site resides in a minor-groove triple helix (Jenkins, Krucinska, McCarty, Bandarian, & Wedekind, 2011; Lund, Chatterjee, Daher, & Walter, 2019). Likewise, it will be interesting to learn if proteins can recognize riboswitches that possess a major-groove triple helix. Overall, riboswitches show how triple helices play an important role in sensing ligands and in regulating expression of prokaryotic genes.

3.4 | RNA triple helix as a stability element

RNA triple helices have been cleverly co-opted by viruses to stabilize RNA. The first example was a triple helix found in the polyadenylated nuclear (PAN) RNA, which is a highly abundant nuclear lncRNA expressed by the Kaposi's sarcoma-associated herpesvirus (KSHV) during the lytic phase of infection and plays various roles in gene expression (Conrad, 2016; Mitton-Fry et al., 2010; Sun, Lin, Gradoville, & Miller, 1996; Zhong, Wang, Herndier, & Ganem, 1996). The KSHV PAN RNA triple helix resides at the 3′ end and consists of two *cis*-acting RNA elements: A stem-loop structure containing a U-rich internal loop and a 3′-poly(A) tail (Figure 6a). An X-ray crystal structure of the KSHV PAN RNA triple helix shows the U-rich internal loop engaged with oligo A_9, forming five U•A-U major-groove base triples and three A-minor base triples (Figure 6a; Mitton-Fry et al., 2010). This extensive network of tertiary interactions protects the poly(A) tail and inhibits rapid nuclear RNA decay, establishing one mechanism by which PAN RNA accumulates to high levels in KSHV-infected cells (Conrad, 2016; Conrad, Mili, Marshall, Shu, & Steitz, 2006; Conrad, Shu, Uyhazi, & Steitz, 2007; Conrad & Steitz, 2005; Mitton-Fry et al., 2010; Sun et al., 1996; Zhong et al., 1996). Notably, the triple-helical structure itself, without any protein cofactors, is necessary and sufficient to inhibit deadenylation catalyzed by purified recombinant PARN (poly(A)-specific ribonuclease) in an in vitro system (Conrad et al., 2006).

Collectively, the KSHV PAN RNA triple helix revealed a novel mechanism by which a viral lncRNA counteracted nuclear RNA decay. Because the mechanism was originally found in a viral lncRNA, this work prompted the question: Do other viral and host RNAs harbor triple-helical RNA stability elements?

Indeed, similar stability elements abound in nature, for more than 200 have been computationally identified in (a) lncRNAs expressed by dsDNA viruses, the MALAT1 lncRNA in vertebrates and likely the MENβ lncRNA in mammals; (b) genomic ssRNA(+) from dicistroviruses; and (c) transposable elements, including those that are transposase mRNAs from plants, fungi, slime mold, and stickleback fish retroviruses (Brown et al., 2012; Tycowski, Shu, Borah, Shi, & Steitz, 2012; Tycowski, Shu, & Steitz, 2016; Wilusz et al., 2012; B. Zhang et al., 2017). Among the 200+ stability elements predicted to date, the functionality of about 10 has been confirmed by their ability to stabilize heterologous intronless β-globin or GFP reporter mRNAs, a function that is likely mediated by formation of a triple helix (Brown et al., 2012; Tycowski et al., 2012, 2016; Wilusz et al., 2012). More interestingly, structural analyses revealed that the stability elements can be classified as single or double domain, whereby each U-rich internal loop represents a domain (Figure 6a,b; Tycowski et al., 2016). Most of the plant transposable elements possess a double-domain stability element (Tycowski et al., 2016). Here, the upper domain resembles the canonical KSHV PAN U-rich stem-loop whereas the lower domain shows two notable structural differences: A 3- or 4-nucleotide-long bulge and the A-minor stem interrupted by a bulge or an internal loop (Tycowski et al., 2016). Like the single-domain stability elements, the poly(A) tail is predicted to interact with both U-rich internal loops, although mutational studies indicate the upper domain of the TWIFB1_OSa structure is responsible for most stabilization activity (Figure 6b; Tycowski et al., 2016). Currently, there is no 3D structure of a double-domain stability element; therefore, it will be interesting to learn the structural significance of the upper domain over the lower domain and if the poly(A) tail engages in tertiary interactions with the stem connecting the upper and lower domains.

Among the 200+ stability elements discovered to date, the MALAT1 and MENβ structures are distinctly different from all others (Figure 6). The MALAT1 and MENβ lncRNAs undergo 3′-end processing by RNase P due to the presence of tRNA-like structures in their transcripts and the resulting mature forms of MALAT1 and MENβ terminate with genomically encoded A-rich tracts rather than 3′-poly(A) tails (Sunwoo et al., 2009; Wilusz, Freier, & Spector, 2008). The single-domain MALAT1 and MENβ stability elements have U-rich internal loops uniquely interrupted by G and C nucleotides that interact with the complementary nucleotides in the downstream A-rich tract so that the triple helices have a blunt end, rather than a 3′-poly(A) tail overhang predicted for others (Figure 6; Brown et al., 2012, 2014; Wilusz et al., 2012). The blunt-ended triple helix of MALAT1 effectively inhibits the rapid phase of nuclear RNA decay whereas the KSHV PAN RNA triple helix only reduces the rapid phase according to a cell-based intronless β-globin reporter

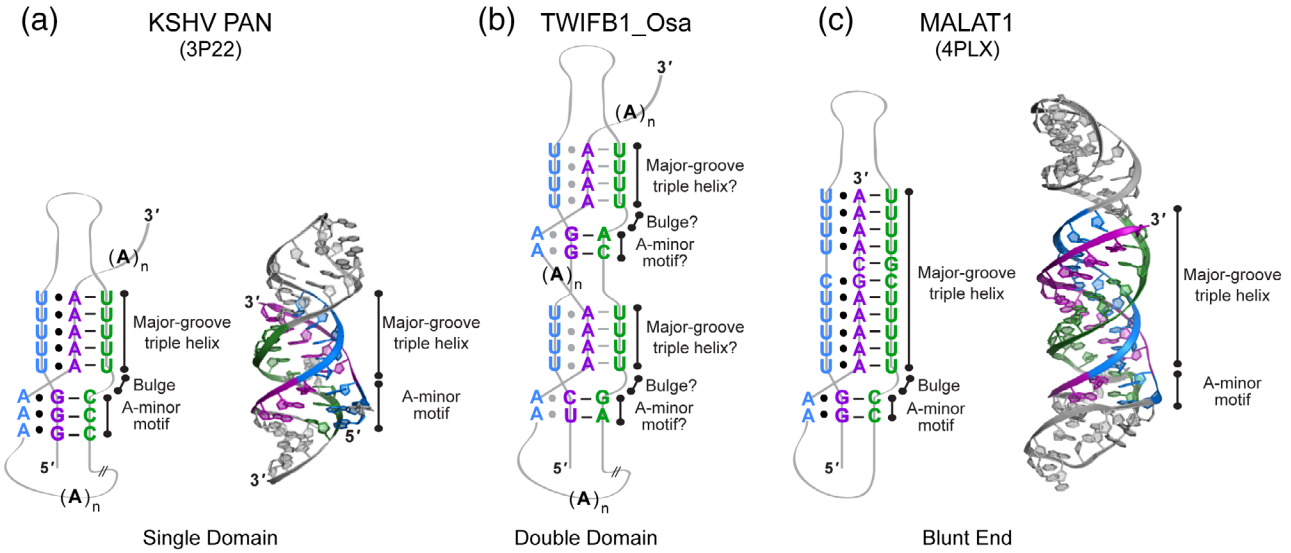

FIGURE 6 Structures of triple helices that function as RNA stability elements. (a) A generalized schematic diagram is shown for a single-domain stability element alongside the X-ray crystal structure of the KSHV PAN RNA triple helix (cartoon representation). Important structural regions are labeled. (b) A generalized schematic diagram is shown for the predicted structure of a double-domain stability element: TWIFB1_Osa. Gray circles (•) and dashed lines (–) indicate putative nucleotide interactions. (c) A generalized schematic diagram and X-ray crystal structure is shown for a blunt-ended RNA triple helix: Human MALAT1 (cartoon representation). The tricolor scheme of strands and symbols for their interactions are described in Figure 1. The PDB IDs are listed below each RNA label

decay assay in HeLa-TetOff cells (Brown et al., 2014; Conrad et al., 2006). However, the decay machinery for the MALAT1 and KSHV PAN triple helices may be different. While KSHV PAN undergoes a deadenylation-dependent decay due to its poly(A) tail, the 3′ end of MALAT1 is sequestered into a blunt-ended triple helix; therefore, it may first require a helicase, such as DHX9, to disrupt the triple helix and/or undergo oligouridylation (Brown et al., 2016b; Jain, Bacolla, Chakraborty, Grosse, & Vasquez, 2010; Wilusz et al., 2012). Moreover, the MALAT1 triple helix interacts with a protein, methyltransferase-like protein 16 (METTL16; Brown et al., 2016b; Warda et al., 2017). METTL16 is an N^6-methyladenosine (m^6A) RNA methyltransferase and how the METTL16-triple helix complex affects the half-life of MALAT1 remains unknown as well as the biological function of the complex itself (Pendleton et al., 2017). A weak m^6A site has been detected in the upper stem of the MALAT1 stability element using miCLIP (m^6A individual-nucleotide resolution crosslinking and RNA immunoprecipitation), although it is unknown if METTL16 catalyzes formation of this m^6A mark and/or recognizes it (Linder et al., 2015; Pendleton et al., 2017). Lastly, another unique function of the MALAT1 triple helix is that it upregulates translation in the context of a GFP reporter system (Wilusz et al., 2012). Therefore, understanding the mechanism of translational upregulation mediated by a triple helix may potentially lead to the discovery of novel triple helices having roles in the cytoplasm.

In summary, triple-helical RNA stability elements exist for multiple classes of RNAs, including those that localize to the nucleus and cytoplasm as well as those expressed by viruses, animals, fungi, and plants. Understanding the structure and function of these unique stability elements has led to novel experimental tools as well as drug targets. For example, the MALAT1 triple helix has been used to study the functional role of the poly(A) tail in transposons and used as a stability tool for RNAs in cell-based systems (Doucet, Wilusz, Miyoshi, Liu, & Moran, 2015; Nissim, Perli, Fridkin, Perez-Pinera, & Lu, 2014; Vogan et al., 2016; Zhan, Xie, Zhou, Liu, & Huang, 2018). Moreover, MALAT1 is upregulated in multiple cancer types and its triple helix is required for this accumulation, making it a potential drug target (Gutschner, Hammerle, & Diederichs, 2013). Most triple-helical RNA stability elements remain uncharacterized and likely hold the potential to revealing more unique insights into the roles of RNA triple helices in biology.

3.5 | Other RNA triple helices

Other RNA triple helices containing major-groove base triples have been observed. Notably, two consecutive U•A-U base triples were observed in an NMR structure of the 7SK stem-loop 1 in complex with a peptide representing the RNA-binding domain of the HIV Tat protein (Pham et al., 2018). Interestingly, arginine sandwich motifs recognize the Hoogsteen face of G in C-G base pairs flanking the U•A-U base triples. A similar mode of recognition of a C-G base pair adjacent to a U•A-U base triple in HIV-1 TAR RNA has been demonstrated for arginine residues in HIV Tat and a lab-evolved RNA recognition motif (Belashov et al., 2018; Pham et al., 2018). Also noteworthy, an X-ray crystal structure of *Campylobacter jejuni* Cas9 in complex with guide RNA and DNA revealed an unusual arrangement of a U•A•G major-groove base triple and an A•A-U minor-groove base triple being interrupted by a base quintuple and an extrahelical residue, A63 (Yamada et al., 2017). Because *C. jejuni* tracrRNA (*trans*-activating CRISPR RNA) lacks two consecutive major-groove base triples, it is not included in the table of triple helices (Table 1). Nonetheless, it is notable that Cas9 does not establish base triple-specific interactions except for an arginine-phosphate backbone contact (Yamada et al., 2017). Rather, the extrahelical base of A63 stacks with a histidine residue and the N1 of A63 forms a hydrogen bond with an asparagine residue (Yamada et al., 2017). Therefore, it is possible that proteins recognize flanking sequences and structures of triple helices instead of the triple helix itself.

Additional RNA triple helices have been reported, although some have only partial triple helix character or there is no 3D structure and/or cell-based compensatory mutagenesis studies performed to validate triple helix. In vitro-selected aptamers having base triples were not discussed in this review because they are non-natural RNAs. Finally, R•D-D triple helices comprised of noncoding RNA and genomic DNA were not discussed because this review is focused on triple helices in which all three strands are RNA.

4 | DISCOVERING RNA TRIPLE HELICES

A long-standing challenge in the field of RNA triple helices is the lack of experimental approaches to unambiguously identify natural RNA triple helices (i.e., the triplexome) rather than rely on their serendipitous discovery upon solving

the 3D structure of an RNA that happens to form a triple helix, such as many of those listed in Table 1. To overcome this technical limitation, another molecule could be designed or adapted to specifically recognize only triple helices and not other nucleic acid structures. Furthermore, the recognition of triple helices could be refined to select triple helices based on strand identity: All DNA, all RNA, or a DNA–RNA hybrid. Regardless of the composition of the triple helix, various molecules could theoretically be adapted for an experimental strategy that specifically recognizes a triple helix, such as nucleic acids, proteins, small molecules, or some combination of the three. The current status and future prospects of these putative triplex-specific binders are discussed below.

4.1 | Nucleic acids

Of all molecules that could specifically recognize a triple helix, nucleic acids may arguably be one of the most challenging from a global discovery perspective. One, the use of a single-stranded oligonucleotide could potentially bind to another single-stranded oligonucleotide, leading to the isolation of a duplex and not the desired triple helix. Two, the sequence of an oligonucleotide will limit binding partners unless universal bases could be exploited for Hoogsteen binding (Hoshika et al., 2019; Rusling et al., 2005). Nonetheless, polyribonucleotide-linked columns have been used as tools for double-helix affinity capture (DAC) via triple helix formation (Flavell & Van Den Berg, 1975; Johnson et al., 1996; Letai et al., 1988; Zuidema, Van den Berg, & Flavell, 1978). Thus, duplexes with a propensity to form triple helices could be identified by eluting duplexes from the column and then subjecting them to high-throughput deep sequencing. Similarly, triplex-forming oligonucleotides (TFOs), which function as the "third strand" and engage duplexes via Hoogsteen interactions, have been developed as a tool to modulate gene expression (see [Bahal, Gupta, and Glazer (2016)] for review). Covalently linking TFOs to crosslinkers, such as psoralen, to selectively pulldown duplexes via triple helix formation has been successful in *Escherichia coli* and human cell extract (Isogawa, Fuchs, & Fujii, 2018).

Aptamers, which are synthetic single-stranded nucleic acids that bind to a specific target, are conceptually another potential strategy. Nucleic acid-based aptamers, typically developed using systematic evolution of ligands by exponential enrichment (SELEX), have been effective at specifically recognizing targets of various sizes and shapes, from small molecules and metal ions to proteins and microorganisms (see [T. Wang, Chen, Larcher, Barrero, and Veedu (2019)] for a review). However, the only aptamer designed to target a specific RNA is HIV-1 TAR RNA, and that aptamer was selected mainly for its sequence complementarity to the TAR loop and not structure (Duconge & Toulme, 1999). Thus, it remains to be tested whether nucleic acid aptamers could specifically recognize the highly electronegative structure of a triple helix (Figure 2). Considering the diverse base triple composition of known triple helices (Table 1), using nucleic acids for the global discovery of triple helices will be more challenging but certainly represent valuable tools for validating specific triple helices in a low-throughput manner.

4.2 | Proteins

Antibodies have the ability to recognize a specific molecule with high affinity. Although nucleic acids are often times weakly immunogenic, several antibodies against triple helices have been reported in the literature, including one that can discriminate between poly(U•A-U) versus poly(U•dA-dT) triple helices (Rainen & Stollar, 1977; Stollar & Raso, 1974; Thomas, Seibold, Adams, & Hess, 1995). Therefore, a straightforward approach to map RNA triple helices would be to perform an immunopurification using an anti-RNA triple helix antibody followed by deep sequencing to identify bound nucleic acids. Considering the diversity of base triples in natural RNA triple helices, it may be necessary to use multiple antibodies or to identify an antibody whose recognition of triple helices is independent of sequence. Another important variable to test would be the number of base triples. Most antibodies are generated against poly(U•A-U) containing dozens or maybe hundreds of base triples whereas most natural RNA triple helices are limited in length to three to six base triples (Table 1). Looking to nature for help would be another possibility, for proteins have been observed to bind to DNA and RNA triple helices (Table 1; Buske, Mattick, & Bailey, 2011). Regardless of the protein used to isolate triple helices, a clever strategy will be needed to bioinformatically determine which strands belong to which triple helix (Russo et al., 2019).

4.3 | Small molecules

As mentioned above (see Section 3.3), riboswitches are the best example in nature of a small molecule engaged with a triple helix. In a non-natural context, more than a dozen small molecules are known to preferentially bind to RNA triple helices over their double helix counterparts or can induce triplex formation: Berberine and analogs (Bhowmik, Das, Hossain, Haq, & Suresh Kumar, 2012; Das, Kumar, Ray, & Maiti, 2003; Sinha & Kumar, 2009), berenil (Pilch, Kirolos, & Breslauer, 1995), coralyne (Sinha & Kumar, 2009), fisetin (Bhuiya, Haque, Goswami, & Das, 2017), luteolin (Tiwari, Haque, Bhuiya, & Das, 2017), neomycin (Arya, Coffee Jr., Willis, & Abramovitch, 2001), palmatine (Sinha & Kumar, 2009), quercetin (Pradhan, Bhuiya, Haque, & Das, 2018), ruthenium(II) complexes (X. J. He & Tan, 2014), sanguinarine (Das et al., 2003) and a benzo[f]quino[3,4-b]quinoxaline derivative conjugated to neomycin (Arya, Xue, & Tennant, 2003; Figure 7a). These molecules generally bind to RNA triple helices with dissociation constants in the nanomolar to low micromolar range. Currently, there are no high-resolution structures of a triple helix in complex with the aforementioned compounds, although various binding modes are predicted, such as intercalation and groove binding (Haq & Ladbury, 2000; Sinha & Kumar, 2009). Regardless of binding mode, these small molecules are rather promiscuous, as they can bind to other noncanonical nucleic acid structures and sometimes cannot distinguish between DNA versus RNA triple helices (Ren & Chaires, 1999). Elucidating the triplex-binding properties of these small molecules holds the potential of exploiting them for the global discovery of triple helices. Such a precedent has been established for the duplex-crosslinker psoralen (AMT) used by PARIS (psoralen analysis of RNA interactions and structures) and LIGR-seq (ligation of interacting RNA followed by high-throughput sequencing) methods to identify double-stranded RNA inside cells and the G-quadruplex-crosslinker BioTASQ used by G4RP-seq (G4-RNA-specific precipitation and sequencing) to capture four-stranded RNA inside cells (Lu et al., 2016; Sharma, Sterne-Weiler, O'Hanlon, & Blencowe, 2016; Yang et al., 2018). These studies provide proof-of-principle that small-molecule crosslinkers can be used to identify multi-stranded RNA structures inside cells.

More recently, two independent studies discovered small molecules that can selectively recognize the MALAT1 triple helix, a structure that represents a unique anti-cancer drug target (Abulwerdi et al., 2019; Donlic et al., 2018). The Hargrove group used an in vitro fluorescence-based assay to show that the compound dubbed DPFp8 (Figure 7b), a diphenylfuran-based derivative, binds to the MALAT1 triple helix with an EC_{50} of 36 nM but no binding to a MALAT1 construct that lacks a triple helix was detected (Donlic et al., 2018). Although DPFp8 is predicted to have a rod-like shape, its binding mode to the MALAT1 triple helix is unknown (Donlic et al., 2018). The LeGrice and Baird groups identified two compounds, dubbed **5** and **16** (Figure 7b), that bind to the MALAT1 triple helix with K_D values of ~2 to 8 μM and a 1:1 stoichiometry of RNA:compound (Abulwerdi et al., 2019). Neither compound appears to bind via intercalation based on results from a dye displacement assay but instead, molecular docking studies predict different groove-binding modes and sites for each compound: Compound **5** via van der Waals interactions along major groove at a central region of triple helix and compound **16** at the surface of minor groove near the terminus of triple helix adjacent to A-minor motif (Figure 6c; Abulwerdi et al., 2019). More importantly, both compounds are functional in mammary tumor organoids, reducing MALAT1 levels by ~50% and branching morphogenesis by ~30% (Abulwerdi et al., 2019). The dynamics of the MALAT1 RNA triple helix in a test tube versus inside a cell is another consideration in drug design (Ageeli, McGovern-Gooch, Kaminska, & Baird, 2019; Yonkunas & Baird, 2019).

Collectively, this body of work further illustrates that (a) RNA triple helices play important biological roles, including in disease states, (b) RNA structures, like proteins, are viable drug targets, and (c) small molecules could be developed as an experimental tool to establish nature's triplexome. A 3D structure of a small molecule in complex with a triple helix will likely open new avenues in designing small molecules for RNA triple helices. Additionally, the recent X-ray crystal structure of a U•A-U-rich triple helix containing 11 consecutive base triples provides a structural platform to model ligand binding (Ruszkowska et al., 2020).

4.4 | Computational predictions

Besides experimental methods, computational strategies have spurred the identification of some triple helices. For example, several lncRNA•gDNA triple helices have been identified using one or more computational approaches, such as LongTarget, Triplexator, TRIPLEXES, and Triplex Domain Finder (Buske, Bauer, Mattick, & Bailey, 2012; S. He, Zhang, Liu, & Zhu, 2015; Kuo et al., 2019; Lin et al., 2019). For intermolecular triple helices like lncRNA•gDNA, computational programs rely on Hoogsteen base-pairing rules or the so-called triple-strand code. The relative stability of all

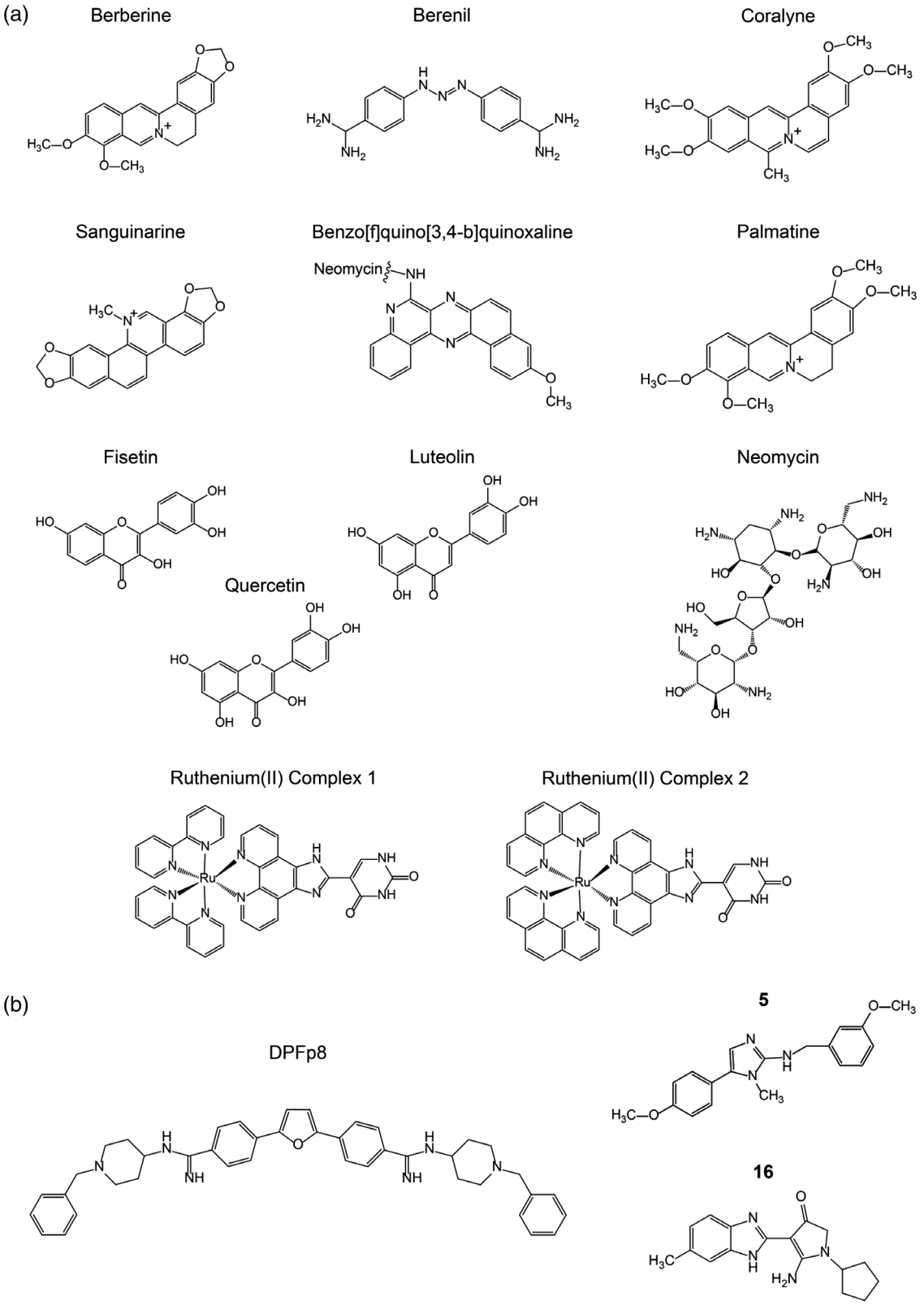

FIGURE 7 Chemical structures of triplex-binding small molecules. Chemical structures are shown for small molecules that (a) broadly recognize RNA triple helices and (b) bind to the MALAT1 RNA triple helix

16 base triples has been quantitatively determined for D•D-D, R•R-R, and R•D-D triple helices, although no universal rules emerge, at least for the 14 noncanonical base triples (Best & Dervan, 1995; Brown et al., 2016a; Kunkler et al., 2019; Mergny et al., 1991). Thus, a new experimental strategy to map R•D-D triple helices inside cells has been

developed, whereby protein-free DNA-associated RNA and RNA-associated DNA is isolated and then subjected to a series of nuclease digests followed by high-throughput sequencing (Senturk Cetin et al., 2019).

For intramolecular triple helices, the computational strategy is not trivial because it involves RNA tertiary structure, which is extremely difficult to accurately predict de novo. Nonetheless, some major-groove triple helices are pseudoknots (see [Peselis and Serganov (2014)] for review); therefore, pseudoknot-predicting algorithms, such as HotKnots, Maximum Weighted Matching method, PKNOTS, and ProbKnot, could be a starting point (Bellaousov & Mathews, 2010; Ren, Rastegari, Condon, & Hoos, 2005; Rivas & Eddy, 1999; Tabaska, Cary, Gabow, & Stormo, 1998). Additionally, many of the riboswitches and triple-helical RNA stability elements have been predicted by computationally searching for conserved structural elements using Infernal or other structural homology-based programs (Nawrocki & Eddy, 2013). For example, the triple-helical RNA stability elements consist of a stem-loop structure containing a U-rich internal loop adjacent to one or more G-C base pairs that facilitate A-minor interactions (Figure 6; Tycowski et al., 2012; Tycowski et al., 2016; B. Zhang et al., 2017). In general, computational approaches can guide researchers to triple helices, although all putative triple helices must undergo experimental validation.

5 | CONCLUSION

Elucidating the biology of characterized RNA triple helices, albeit relatively few to date, illustrates how these non-canonical structures can be utilized by prokaryotes, eukaryotes, and viruses in nearly ubiquitous cellular mechanisms, such as catalysis and ligand binding. Because RNA function usually involves dynamic interactions with protein-binding partners, an important next step is to understand the specific role of RNA triple helices in RNPs. For example, the triple helix in TR is required for telomerase activity but resides outside the active site. Moreover, RNA triple helices represent novel therapeutic targets, for they exist in RNAs having prominent roles in human health, such as TR and the MALAT1 lncRNA in cancer. More RNA triple helices likely exist and have essential roles in biology, including implications in human health. To identify the triplexome, novel methods will need to be developed in accelerating our efforts to understand the structure and function of major-groove RNA triple helices throughout nature. These efforts may advance via insights from nature (e.g., riboswitches or triple-stranded RNA-binding proteins), from molecules developed in the laboratory (e.g., synthetic compounds or antibodies), or from a combination of nature and laboratory. Once a triplexome is established, the biological roles of RNA triple helices can be unraveled.

ACKNOWLEDGMENTS

Thank you to Gregor Blaha, Jacob Hulewicz, and Allen Oliver for their kind assistance during figure preparation and to the Brown laboratory for critically reading the manuscript. This work was supported by the NIH Grant R35GM133696 to J. A. B., the Clare Boothe Luce Program of the Henry Luce Foundation, and startup funds from the University of Notre Dame.

CONFLICT OF INTEREST

The author has declared no conflicts of interest for this article.

ORCID

Jessica A. Brown https://orcid.org/0000-0001-9055-5939

RELATED WIREs ARTICLES

The emerging role of triple helices in RNA biology

RNA triplexes: from structural principles to biological and biotech applications

REFERENCES

Abu Almakarem, A. S., Petrov, A. I., Stombaugh, J., Zirbel, C. L., & Leontis, N. B. (2012). Comprehensive survey and geometric classification of base triples in RNA structures. *Nucleic Acids Research*, *40*(4), 1407–1423. https://doi.org/10.1093/nar/gkr810

Abulwerdi, F. A., Xu, W., Ageeli, A. A., Yonkunas, M. J., Arun, G., Nam, H., ... Le Grice, S. F. J. (2019). Selective small-molecule targeting of a triple helix encoded by the long noncoding RNA, MALAT1. *ACS Chemical Biology*, *14*(2), 223–235. https://doi.org/10.1021/acschembio.8b00807

Adams, P. L., Stahley, M. R., Kosek, A. B., Wang, J., & Strobel, S. A. (2004). Crystal structure of a self-splicing group I intron with both exons. *Nature*, *430*(6995), 45–50. https://doi.org/10.1038/nature02642

Ageeli, A. A., McGovern-Gooch, K. R., Kaminska, M. M., & Baird, N. J. (2019). Finely tuned conformational dynamics regulate the protective function of the lncRNA MALAT1 triple helix. *Nucleic Acids Research*, *47*(3), 1468–1481. https://doi.org/10.1093/nar/gky1171

Arnott, S., & Bond, P. J. (1973). Structures for poly(U)•poly(A)-poly(U) triple-stranded polynucleotides. *Nature: New Biology*, *244*(134), 99–101. https://doi.org/10.1038/newbio244099a0

Arnott, S., Bond, P. J., Selsing, E., & Smith, P. J. (1976). Models of triple-stranded polynucleotides with optimised stereochemistry. *Nucleic Acids Research*, *3*(10), 2459–2470.

Arnott, S., Hukins, D. W., Dover, S. D., Fuller, W., & Hodgson, A. R. (1973). Structures of synthetic polynucleotides in the A-RNA and A'-RNA conformations: X-ray diffraction analyses of the molecular conformations of polyadenylic acid-polyuridylic acid and polyinosinic acid-polycytidylic acid. *Journal of Molecular Biology*, *81*(2), 107–122. https://doi.org/10.1016/0022-2836(73)90183-6

Arya, D. P., Coffee, R. L., Jr., Willis, B., & Abramovitch, A. I. (2001). Aminoglycoside-nucleic acid interactions: Remarkable stabilization of DNA and RNA triple helices by neomycin. *Journal of the American Chemical Society*, *123*(23), 5385–5395.

Arya, D. P., Xue, L., & Tennant, P. (2003). Combining the best in triplex recognition: Synthesis and nucleic acid binding of a BQQ-neomycin conjugate. *Journal of the American Chemical Society*, *125*(27), 8070–8071. https://doi.org/10.1021/ja034241t

Asensio, J. L., Lane, A. N., Dhesi, J., Bergqvist, S., & Brown, T. (1998). The contribution of cytosine protonation to the stability of parallel DNA triple helices. *Journal of Molecular Biology*, *275*(5), 811–822. https://doi.org/10.1006/jmbi.1997.1520

Aytenfisu, A. H., Liberman, J. A., Wedekind, J. E., & Mathews, D. H. (2015). Molecular mechanism for $PreQ_1$-II riboswitch function revealed by molecular dynamics. *RNA*, *21*(11), 1898–1907. https://doi.org/10.1261/rna.051367.115

Bahal, R., Gupta, A., & Glazer, P. M. (2016). Precise genome modification using triplex forming oligonucleotides and peptide nucleic acids. In T. Cathomen, M. Hirsch, & M. Porteus (Eds.), *Genome Editing. Advances in Experimental Medicine and Biology* (pp. 93–110). New York, NY: Springer.

Bao, P., Boon, K. L., Will, C. L., Hartmuth, K., & Luhrmann, R. (2018). Multiple RNA-RNA tertiary interactions are dispensable for formation of a functional U2/U6 RNA catalytic core in the spliceosome. *Nucleic Acids Research*, *46*(22), 12126–12138. https://doi.org/10.1093/nar/gky966

Belashov, I. A., Crawford, D. W., Cavender, C. E., Dai, P., Beardslee, P. C., Mathews, D. H., ... Wedekind, J. E. (2018). Structure of HIV TAR in complex with a lab-evolved RRM provides insight into duplex RNA recognition and synthesis of a constrained peptide that impairs transcription. *Nucleic Acids Research*, *46*(13), 6401–6415. https://doi.org/10.1093/nar/gky529

Bellaousov, S., & Mathews, D. H. (2010). ProbKnot: Fast prediction of RNA secondary structure including pseudoknots. *RNA*, *16*(10), 1870–1880. https://doi.org/10.1261/rna.2125310

Bertram, K., Agafonov, D. E., Liu, W. T., Dybkov, O., Will, C. L., Hartmuth, K., ... Luhrmann, R. (2017). Cryo-EM structure of a human spliceosome activated for step 2 of splicing. *Nature*, *542*(7641), 318–323. https://doi.org/10.1038/nature21079

Best, G. C., & Dervan, P. B. (1995). Energetics of formation of sixteen triple helical complexes which vary at a single position within a pyrimidine motif. *Journal of the American Chemical Society*, *117*, 1187–1193.

Bhowmik, D., Das, S., Hossain, M., Haq, L., & Suresh Kumar, G. (2012). Biophysical characterization of the strong stabilization of the RNA triplex poly(U)•poly(A)-poly(U) by 9-*O*-(omega-amino) alkyl ether berberine analogs. *PLoS One*, *7*(5), e37939. https://doi.org/10.1371/journal.pone.0037939

Bhuiya, S., Haque, L., Goswami, R., & Das, S. (2017). Multispectroscopic and theoretical exploration of the comparative binding aspects of bioflavonoid fisetin with triple- and double-helical forms of RNA. *Journal of Physical Chemistry B*, *121*(49), 11037–11052. https://doi.org/10.1021/acs.jpcb.7b07972

Boulanger, S. C., Belcher, S. M., Schmidt, U., Dib-Hajj, S. D., Schmidt, T., & Perlman, P. S. (1995). Studies of point mutants define three essential paired nucleotides in the domain 5 substructure of a group II intron. *Molecular and Cellular Biology*, *15*(8), 4479–4488. https://doi.org/10.1128/mcb.15.8.4479

Breaker, R. R. (2012). Riboswitches and the RNA world. *Cold Spring Harbor Perspectives in Biology*, *4*(2), a003566. https://doi.org/10.1101/cshperspect.a003566

Breaker, R. R. (2018). Riboswitches and translation control. *Cold Spring Harbor Perspectives in Biology*, *10*(11), a032797. https://doi.org/10.1101/cshperspect.a032797

Brown, J. A., Bulkley, D., Wang, J., Valenstein, M. L., Yario, T. A., Steitz, T. A., & Steitz, J. A. (2014). Structural insights into the stabilization of MALAT1 noncoding RNA by a bipartite triple helix. *Nature Structural & Molecular Biology*, *21*(7), 633–640. https://doi.org/10.1038/nsmb.2844

Brown, J. A., Kinzig, C. G., DeGregorio, S. J., & Steitz, J. A. (2016a). Hoogsteen-position pyrimidines promote the stability and function of the MALAT1 RNA triple helix. *RNA*, *22*(5), 743–749. https://doi.org/10.1261/rna.055707.115

Brown, J. A., Kinzig, C. G., DeGregorio, S. J., & Steitz, J. A. (2016b). Methyltransferase-like protein 16 binds the 3′-terminal triple helix of MALAT1 long noncoding RNA. *Proceedings of the National Academy of Sciences of the United States of America*, *113*(49), 14013–14018. https://doi.org/10.1073/pnas.1614759113

Brown, J. A., Valenstein, M. L., Yario, T. A., Tycowski, K. T., & Steitz, J. A. (2012). Formation of triple-helical structures by the 3′-end sequences of MALAT1 and MENβ noncoding RNAs. *Proceedings of the National Academy of Sciences of the United States of America*, *109*(47), 19202–19207. https://doi.org/10.1073/pnas.1217338109

Buske, F. A., Bauer, D. C., Mattick, J. S., & Bailey, T. L. (2012). Triplexator: Detecting nucleic acid triple helices in genomic and transcriptomic data. *Genome Research*, *22*(7), 1372–1381. https://doi.org/10.1101/gr.130237.111

Buske, F. A., Mattick, J. S., & Bailey, T. L. (2011). Potential *in vivo* roles of nucleic acid triple helices. *RNA Biology*, *8*(3), 427–439.

Callahan, D. E., Trapane, T. L., Miller, P. S., Ts'o, P. O., & Kan, L. S. (1991). Comparative circular dichroism and fluorescence studies of oligodeoxyribonucleotide and oligodeoxyribonucleoside methylphosphonate pyrimidine strands in duplex and triplex formation. *Biochemistry*, *30*(6), 1650–1655. https://doi.org/10.1021/bi00220a030

Cash, D. D., Cohen-Zontag, O., Kim, N. K., Shefer, K., Brown, Y., Ulyanov, N. B., ... Feigon, J. (2013). Pyrimidine motif triple helix in the *Kluyveromyces lactis* telomerase RNA pseudoknot is essential for function *in vivo*. *Proceedings of the National Academy of Sciences of the United States of America*, *110*(27), 10970–10975. https://doi.org/10.1073/pnas.13095901101309590110

Cash, D. D., & Feigon, J. (2017). Structure and folding of the *Tetrahymena* telomerase RNA pseudoknot. *Nucleic Acids Research*, *45*(1), 482–495. https://doi.org/10.1093/nar/gkw1153

Chan, R. T., Peters, J. K., Robart, A. R., Wiryaman, T., Rajashankar, K. R., & Toor, N. (2018). Structural basis for the second step of group II intron splicing. *Nature Communications*, *9*(1), 4676. https://doi.org/10.1038/s41467-018-06678-0

Chandrasekaran, R., Giacometti, A., & Arnott, S. (2000). Structure of poly(U)•poly(A)-poly(U). *Journal of Biomolecular Structure & Dynamics*, *17*(6), 1023–1034. https://doi.org/10.1080/07391102.2000.10506590

Chen, B., Zuo, X., Wang, Y. X., & Dayie, T. K. (2012). Multiple conformations of SAM-II riboswitch detected with SAXS and NMR spectroscopy. *Nucleic Acids Research*, *40*(7), 3117–3130. https://doi.org/10.1093/nar/gkr1154

Chen, G., Chang, K. Y., Chou, M. Y., Bustamante, C., & Tinoco, I., Jr. (2009). Triplex structures in an RNA pseudoknot enhance mechanical stability and increase efficiency of −1 ribosomal frameshifting. *Proceedings of the National Academy of Sciences of the United States of America*, *106*(31), 12706–12711. https://doi.org/10.1073/pnas.0905046106

Chen, J. L., Blasco, M. A., & Greider, C. W. (2000). Secondary structure of vertebrate telomerase RNA. *Cell*, *100*(5), 503–514. https://doi.org/10.1016/s0092-8674(00)80687-x

Conrad, N. K. (2014). The emerging role of triple helices in RNA biology. *WIREs RNA*, *5*(1), 15–29. https://doi.org/10.1002/wrna.1194

Conrad, N. K. (2016). New insights into the expression and functions of the Kaposi's sarcoma-associated herpesvirus long noncoding PAN RNA. *Virus Research*, *212*, 53–63. https://doi.org/10.1016/j.virusres.2015.06.012

Conrad, N. K., Mili, S., Marshall, E. L., Shu, M. D., & Steitz, J. A. (2006). Identification of a rapid mammalian deadenylation-dependent decay pathway and its inhibition by a viral RNA element. *Molecular Cell*, *24*(6), 943–953. https://doi.org/10.1016/j.molcel.2006.10.029

Conrad, N. K., Shu, M. D., Uyhazi, K. E., & Steitz, J. A. (2007). Mutational analysis of a viral RNA element that counteracts rapid RNA decay by interaction with the polyadenylate tail. *Proceedings of the National Academy of Sciences of the United States of America*, *104*(25), 10412–10417. https://doi.org/10.1073/pnas.0704187104

Conrad, N. K., & Steitz, J. A. (2005). A Kaposi's sarcoma virus RNA element that increases the nuclear abundance of intronless transcripts. *EMBO Journal*, *24*(10), 1831–1841. https://doi.org/10.1038/sj.emboj.7600662

Das, S., Kumar, G. S., Ray, A., & Maiti, M. (2003). Spectroscopic and thermodynamic studies on the binding of sanguinarine and berberine to triple and double helical DNA and RNA structures. *Journal of Biomolecular Structure & Dynamics*, *20*(5), 703–714. https://doi.org/10.1080/07391102.2003.10506887

Devi, G., Zhou, Y., Zhong, Z., Toh, D. F., & Chen, G. (2015). RNA triplexes: From structural principles to biological and biotech applications. *WIREs RNA*, *6*(1), 111–128. https://doi.org/10.1002/wrna.1261

Donlic, A., Morgan, B. S., Xu, J. L., Liu, A., Roble, C., Jr., & Hargrove, A. E. (2018). Discovery of small molecule ligands for MALAT1 by tuning an RNA-binding scaffold. *Angewandte Chemie (International Edition in English)*, *57*(40), 13242–13247. https://doi.org/10.1002/anie.201808823

Doucet, A. J., Wilusz, J. E., Miyoshi, T., Liu, Y., & Moran, J. V. (2015). A 3′- poly(A) tract is required for LINE-1 retrotransposition. *Molecular Cell*, *60*(5), 728–741. https://doi.org/10.1016/j.molcel.2015.10.012

Drew, H. R., Wing, R. M., Takano, T., Broka, C., Tanaka, S., Itakura, K., & Dickerson, R. E. (1981). Structure of a B-DNA dodecamer: Conformation and dynamics. *Proceedings of the National Academy of Sciences of the United States of America*, *78*(4), 2179–2183. https://doi.org/10.1073/pnas.78.4.2179

Duconge, F., & Toulme, J. J. (1999). *In vitro* selection identifies key determinants for loop-loop interactions: RNA aptamers selective for the TAR RNA element of HIV-1. *RNA*, *5*(12), 1605–1614. https://doi.org/10.1017/s1355838299991318

Dutta, D., Belashov, I. A., & Wedekind, J. E. (2018). Coupling green fluorescent protein expression with chemical modification to probe functionally relevant riboswitch conformations in live bacteria. *Biochemistry*, *57*(31), 4620–4628. https://doi.org/10.1021/acs.biochem.8b00316

Dutta, D., & Wedekind, J. E. (2019). Nucleobase mutants of a bacterial $PreQ_1$-II riboswitch that uncouple metabolite sensing from gene regulation. *Journal of Biological Chemistry*, *295*, 2555–2567. https://doi.org/10.1074/jbc.RA119.010755

Escude, C., Francois, J. C., Sun, J. S., Ott, G., Sprinzl, M., Garestier, T., & Helene, C. (1993). Stability of triple helices containing RNA and DNA strands: Experimental and molecular modeling studies. *Nucleic Acids Research*, *21*(24), 5547–5553. https://doi.org/10.1093/nar/21.24.5547

Eysmont, K., Matylla-Kulinska, K., Jaskulska, A., Magnus, M., & Konarska, M. M. (2019). Rearrangements within the U6 snRNA core during the transition between the two catalytic steps of splicing. *Molecular Cell*, *75*(3), 538–548.e533. https://doi.org/10.1016/j.molcel.2019.05.018

Felsenfeld, G., Davies, D. R., & Rich, A. (1957). Formation of a 3-stranded polynucleotide molecule. *Journal of the American Chemical Society*, *79*(8), 2023–2024.

Fica, S. M., Mefford, M. A., Piccirilli, J. A., & Staley, J. P. (2014). Evidence for a group II intron-like catalytic triplex in the spliceosome. *Nature Structural & Molecular Biology*, *21*(5), 464–471. https://doi.org/10.1038/nsmb.2815

Fica, S. M., Tuttle, N., Novak, T., Li, N. S., Lu, J., Koodathingal, P., … Piccirilli, J. A. (2013). RNA catalyses nuclear pre-mRNA splicing. *Nature*, *503*(7475), 229–234. https://doi.org/10.1038/nature12734

Firdaus-Raih, M., Harrison, A. M., Willett, P., & Artymiuk, P. J. (2011). Novel base triples in RNA structures revealed by graph theoretical searching methods. *BMC Bioinformatics*, *12*(Suppl 13), S2. https://doi.org/10.1186/1471-2105-12-S13-S2

Flavell, R. A., & van den Berg, F. M. (1975). The isolation of duplex DNA containing (dA-dT) clusters by affinity chromatography on poly(U) sephadex. *FEBS Letters*, *58*(1), 90–93. https://doi.org/10.1016/0014-5793(75)80232-8

Galej, W. P., Toor, N., Newman, A. J., & Nagai, K. (2018). Molecular mechanism and evolution of nuclear pre-mRNA and group II intron splicing: Insights from cryo-electron microscopy structures. *Chemical Reviews*, *118*(8), 4156–4176. https://doi.org/10.1021/acs.chemrev.7b00499

Gilbert, S. D., Rambo, R. P., Van Tyne, D., & Batey, R. T. (2008). Structure of the SAM-II riboswitch bound to *S*-adenosylmethionine. *Nature Structural & Molecular Biology*, *15*(2), 177–182. https://doi.org/10.1038/nsmb.1371

Gordon, P. M., Fong, R., & Piccirilli, J. A. (2007). A second divalent metal ion in the group II intron reaction center. *Chemistry & Biology*, *14*(6), 607–612. https://doi.org/10.1016/j.chembiol.2007.05.008

Gordon, P. M., & Piccirilli, J. A. (2001). Metal ion coordination by the AGC triad in domain 5 contributes to group II intron catalysis. *Nature Structural Biology*, *8*(10), 893–898. https://doi.org/10.1038/nsb1001-893

Gordon, P. M., Sontheimer, E. J., & Piccirilli, J. A. (2000). Metal ion catalysis during the exon-ligation step of nuclear pre-mRNA splicing: Extending the parallels between the spliceosome and group II introns. *RNA*, *6*(2), 199–205. https://doi.org/10.1017/s1355838200992069

Greider, C. W., & Blackburn, E. H. (1989). A telomeric sequence in the RNA of *Tetrahymena* telomerase required for telomere repeat synthesis. *Nature*, *337*(6205), 331–337. https://doi.org/10.1038/337331a0

Gutschner, T., Hammerle, M., & Diederichs, S. (2013). MALAT1—A paradigm for long noncoding RNA function in cancer. *Journal of Molecular Medicine (Berlin, Germany)*, *91*(7), 791–801. https://doi.org/10.1007/s00109-013-1028-y

Haack, D. B., Yan, X., Zhang, C., Hingey, J., Lyumkis, D., Baker, T. S., & Toor, N. (2019). Cryo-EM structures of a group II intron reverse splicing into DNA. *Cell*, *178*(3), 612–623.e612. https://doi.org/10.1016/j.cell.2019.06.035

Haller, A., Rieder, U., Aigner, M., Blanchard, S. C., & Micura, R. (2011). Conformational capture of the SAM-II riboswitch. *Nature Chemical Biology*, *7*(6), 393–400. https://doi.org/10.1038/nchembio.562

Hang, J., Wan, R., Yan, C., & Shi, Y. (2015). Structural basis of pre-mRNA splicing. *Science*, *349*(6253), 1191–1198. https://doi.org/10.1126/science.aac8159

Haq, I., & Ladbury, J. (2000). Drug-DNA recognition: Energetics and implications for design. *Journal of Molecular Recognition*, *13*(4), 188–197. https://doi.org/10.1002/1099-1352(200007/08)13:4<188::AID-JMR503>3.0.CO;2-1

He, S., Zhang, H., Liu, H., & Zhu, H. (2015). LongTarget: A tool to predict lncRNA DNA-binding motifs and binding sites via Hoogsteen base-pairing analysis. *Bioinformatics*, *31*(2), 178–186. https://doi.org/10.1093/bioinformatics/btu643

He, X. J., & Tan, L. F. (2014). Interactions of octahedral ruthenium(II) polypyridyl complexes with the RNA triplex poly(U)•poly(A)-poly(U) effect on the third-strand stabilization. *Inorganic Chemistry*, *53*(20), 11152–11159. https://doi.org/10.1021/ic5017565

Hoogsteen, K. (1959). The crystal and molecular structure of a hydrogen-bonded complex between 1-methylthymine and 9-methyladenine. *Acta Crystallographica*, *12*, 822–823.

Holbrook, S. R., Sussman, J. L., Warrant, R. W., & Kim, S. H. (1978). Crystal structure of yeast phenylalanine transfer RNA. II. Structural features and functional implications. *Journal of Molecular Biology*, *123*(4), 631–660. https://doi.org/10.1016/0022-2836(78)90210-3

Hoshika, S., Leal, N. A., Kim, M. J., Kim, M. S., Karalkar, N. B., Kim, H. J., … Benner, S. A. (2019). Hachimoji DNA and RNA: A genetic system with eight building blocks. *Science*, *363*(6429), 884–887. https://doi.org/10.1126/science.aat0971

Huang, J., Brown, A. F., Wu, J., Xue, J., Bley, C. J., Rand, D. P., … Lei, M. (2014). Structural basis for protein-RNA recognition in telomerase. *Nature Structural & Molecular Biology*, *21*(6), 507–512. https://doi.org/10.1038/nsmb.2819

Huang, L., & Lilley, D. M. J. (2018). Structure and ligand binding of the SAM-V riboswitch. *Nucleic Acids Research*, *46*(13), 6869–6879. https://doi.org/10.1093/nar/gky520

Huang, L., Wang, J., Wilson, T. J., & Lilley, D. M. J. (2017). Structure of the guanidine III riboswitch. *Cell Chemical Biology*, *24*(11), 1407–1415.e1402. https://doi.org/10.1016/j.chembiol.2017.08.021

Isogawa, A., Fuchs, R. P., & Fujii, S. (2018). Versatile and efficient chromatin pull-down methodology based on DNA triple helix formation. *Scientific Reports*, *8*(1), 5925. https://doi.org/10.1038/s41598-018-24417-9

Jain, A., Bacolla, A., Chakraborty, P., Grosse, F., & Vasquez, K. M. (2010). Human DHX9 helicase unwinds triple-helical DNA structures. *Biochemistry*, *49*(33), 6992–6999. https://doi.org/10.1021/bi100795m

James, P. L., Brown, T., & Fox, K. R. (2003). Thermodynamic and kinetic stability of intermolecular triple helices containing different proportions of C^+•G-C and T•A-T triplets. *Nucleic Acids Research*, *31*(19), 5598–5606.

Jenkins, J. L., Krucinska, J., McCarty, R. M., Bandarian, V., & Wedekind, J. E. (2011). Comparison of a $PreQ_1$ riboswitch aptamer in metabolite-bound and free states with implications for gene regulation. *Journal of Biological Chemistry*, *286*(28), 24626–24637. https://doi.org/10.1074/jbc.M111.230375

Jiang, J., Chan, H., Cash, D. D., Miracco, E. J., Ogorzalek Loo, R. R., Upton, H. E., … Feigon, J. (2015). Structure of *Tetrahymena* telomerase reveals previously unknown subunits, functions, and interactions. *Science*, *350*(6260), aab4070. https://doi.org/10.1126/science.aab4070

Johnson, A. F., Wang, R., Ji, H., Chen, D., Guilfoyle, R. A., & Smith, L. M. (1996). Purification of single-stranded M13 DNA by cooperative triple-helix-mediated affinity capture. *Analytical Biochemistry*, *234*(1), 83–95. https://doi.org/10.1006/abio.1996.0053

Jones, C. P., & Ferre-D'Amare, A. R. (2017). Long-range interactions in riboswitch control of gene expression. *Annual Review of Biophysics*, *46*, 455–481. https://doi.org/10.1146/annurev-biophys-070816-034042

Kalwa, M., Hanzelmann, S., Otto, S., Kuo, C. C., Franzen, J., Joussen, S., ... Wagner, W. (2016). The lncRNA HOTAIR impacts on mesenchymal stem cells via triple helix formation. *Nucleic Acids Research*, *44*(22), 10631–10643. https://doi.org/10.1093/nar/gkw802

Kang, M., Eichhorn, C. D., & Feigon, J. (2014). Structural determinants for ligand capture by a class II $PreQ_1$ riboswitch. *Proceedings of the National Academy of Sciences of the United States of America*, *111*(6), E663–E671. https://doi.org/10.1073/pnas.1400126111

Kim, N. K., Zhang, Q., Zhou, J., Theimer, C. A., Peterson, R. D., & Feigon, J. (2008). Solution structure and dynamics of the wild-type pseudoknot of human telomerase RNA. *Journal of Molecular Biology*, *384*(5), 1249–1261. https://doi.org/10.1016/j.jmb.2008.10.005

Kunkler, C. N., Hulewicz, J. P., Hickman, S. C., Wang, M. C., McCown, P. J., & Brown, J. A. (2019). Stability of an RNA•DNA-DNA triple helix depends on base triplet composition and length of the RNA third strand. *Nucleic Acids Research*, *47*(14), 7213–7222. https://doi.org/10.1093/nar/gkz573

Kuo, C. C., Hanzelmann, S., Senturk Cetin, N., Frank, S., Zajzon, B., Derks, J. P., ... Costa, I. G. (2019). Detection of RNA-DNA binding sites in long noncoding RNAs. *Nucleic Acids Research*, *47*(6), e32. https://doi.org/10.1093/nar/gkz037

Lee, E. R., Baker, J. L., Weinberg, Z., Sudarsan, N., & Breaker, R. R. (2010). An allosteric self-splicing ribozyme triggered by a bacterial second messenger. *Science*, *329*(5993), 845–848. https://doi.org/10.1126/science.1190713

Leitner, D., Schroder, W., & Weisz, K. (2000). Influence of sequence-dependent cytosine protonation and methylation on DNA triplex stability. *Biochemistry*, *39*(19), 5886–5892.

Lescoute, A., & Westhof, E. (2006). The A-minor motifs in the decoding recognition process. *Biochimie*, *88*(8), 993–999. https://doi.org/10.1016/j.biochi.2006.05.018

Letai, A. G., Palladino, M. A., Fromm, E., Rizzo, V., & Fresco, J. R. (1988). Specificity in formation of triple-stranded nucleic acid helical complexes: Studies with agarose-linked polyribonucleotide affinity columns. *Biochemistry*, *27*(26), 9108–9112. https://doi.org/10.1021/bi00426a007

Levene, P. A., Bass, L. W., & Simms, H. S. (1926). The ionization of pyrimidines in relation to the structure of pyrimidine nucleosides. *Journal of Biological Chemistry*, *70*, 229–241.

Li, Y., Syed, J., & Sugiyama, H. (2016). RNA-DNA triplex formation by long noncoding RNAs. *Cell Chemical Biology*, *23*(11), 1325–1333. https://doi.org/10.1016/j.chembiol.2016.09.011

Liberman, J. A., Salim, M., Krucinska, J., & Wedekind, J. E. (2013). Structure of a class II $PreQ_1$ riboswitch reveals ligand recognition by a new fold. *Nature Chemical Biology*, *9*(6), 353–355. https://doi.org/10.1038/nchembio.1231

Liberman, J. A., Suddala, K. C., Aytenfisu, A., Chan, D., Belashov, I. A., Salim, M., ... Wedekind, J. E. (2015). Structural analysis of a class III $PreQ_1$ riboswitch reveals an aptamer distant from a ribosome-binding site regulated by fast dynamics. *Proceedings of the National Academy of Sciences of the United States of America*, *112*(27), E3485–E3494. https://doi.org/10.1073/pnas.1503955112

Lin, J., Wen, Y., He, S., Yang, X., Zhang, H., & Zhu, H. (2019). Pipelines for cross-species and genome-wide prediction of long noncoding RNA binding. *Nature Protocols*, *14*(3), 795–818. https://doi.org/10.1038/s41596-018-0115-5

Linder, B., Grozhik, A. V., Olarerin-George, A. O., Meydan, C., Mason, C. E., & Jaffrey, S. R. (2015). Single-nucleotide-resolution mapping of m^6A and m^6Am throughout the transcriptome. *Nature Methods*, *12*(8), 767–772. https://doi.org/10.1038/nmeth.3453

Lingner, J., Hughes, T. R., Shevchenko, A., Mann, M., Lundblad, V., & Cech, T. R. (1997). Reverse transcriptase motifs in the catalytic subunit of telomerase. *Science*, *276*(5312), 561–567. https://doi.org/10.1126/science.276.5312.561

Liu, F., & Theimer, C. A. (2012). Telomerase activity is sensitive to subtle perturbations of the TLC1 pseudoknot 3′ stem and tertiary structure. *Journal of Molecular Biology*, *423*(5), 719–735. https://doi.org/10.1016/j.jmb.2012.08.025

Lu, Z., Zhang, Q. C., Lee, B., Flynn, R. A., Smith, M. A., Robinson, J. T., ... Chang, H. Y. (2016). RNA duplex map in living cells reveals higher-order transcriptome structure. *Cell*, *165*(5), 1267–1279. https://doi.org/10.1016/j.cell.2016.04.028

Lund, P. E., Chatterjee, S., Daher, M., & Walter, N. G. (2019). Protein unties the pseudoknot: S1-mediated unfolding of RNA higher order structure. *Nucleic Acids Research*, *48*, 2107–2125. https://doi.org/10.1093/nar/gkz1166

Marcia, M., & Pyle, A. M. (2012). Visualizing group II intron catalysis through the stages of splicing. *Cell*, *151*(3), 497–507. https://doi.org/10.1016/j.cell.2012.09.033

Marcia, M., & Pyle, A. M. (2014). Principles of ion recognition in RNA: Insights from the group II intron structures. *RNA*, *20*(4), 516–527. https://doi.org/10.1261/rna.043414.113

McCown, P. J., Corbino, K. A., Stav, S., Sherlock, M. E., & Breaker, R. R. (2017). Riboswitch diversity and distribution. *RNA*, *23*(7), 995–1011. https://doi.org/10.1261/rna.061234.117

McCown, P. J., Liang, J. J., Weinberg, Z., & Breaker, R. R. (2014). Structural, functional, and taxonomic diversity of three $PreQ_1$ riboswitch classes. *Chemistry & Biology*, *21*(7), 880–889. https://doi.org/10.1016/j.chembiol.2014.05.015

McCown, P. J., Ruszkowska, A., Kunkler, C. N., Breger, K., Hulewicz, J. P., Wang, M. C., ... Brown, J. A. (2020). Modified ribonucleosides in biology. *WIREs RNA,* e1595. https://doi.org/10.1002/wrna.1595

Mefford, M. A., & Staley, J. P. (2009). Evidence that U2/U6 helix I promotes both catalytic steps of pre-mRNA splicing and rearranges in between these steps. *RNA*, *15*(7), 1386–1397. https://doi.org/10.1261/rna.1582609

Mergny, J. L., Sun, J. S., Rougee, M., Montenay-Garestier, T., Barcelo, F., Chomilier, J., & Helene, C. (1991). Sequence specificity in triple-helix formation: Experimental and theoretical studies of the effect of mismatches on triplex stability. *Biochemistry*, *30*(40), 9791–9798. https://doi.org/10.1021/bi00104a031

Meyer, M. M., Roth, A., Chervin, S. M., Garcia, G. A., & Breaker, R. R. (2008). Confirmation of a second natural $PreQ_1$ aptamer class in *Streptococcaceae* bacteria. *RNA*, *14*(4), 685–695. https://doi.org/10.1261/rna.937308

Mihalusova, M., Wu, J. Y., & Zhuang, X. (2011). Functional importance of telomerase pseudoknot revealed by single-molecule analysis. *Proceedings of the National Academy of Sciences of the United States of America*, *108*(51), 20339–20344. https://doi.org/10.1073/pnas.1017686108

Mitton-Fry, R. M., DeGregorio, S. J., Wang, J., Steitz, T. A., & Steitz, J. A. (2010). Poly(A) tail recognition by a viral RNA element through assembly of a triple helix. *Science, 330*(6008), 1244–1247. doi: https://doi.org/10.1126/science.1195858

Mondal, T., Subhash, S., Vaid, R., Enroth, S., Uday, S., Reinius, B., ... Kanduri, C. (2015). MEG3 long noncoding RNA regulates the TGFβ-pathway genes through formation of RNA-DNA triplex structures. *Nature Communications*, *6*, 7743. https://doi.org/10.1038/ncomms8743

Morgan, A. R., & Wells, R. D. (1968). Specificity of the three-stranded complex formation between double-stranded DNA and single-stranded RNA containing repeating nucleotide sequences. *Journal of Molecular Biology*, *37*(1), 63–80.

Nakamura, T. M., Morin, G. B., Chapman, K. B., Weinrich, S. L., Andrews, W. H., Lingner, J., ... Cech, T. R. (1997). Telomerase catalytic subunit homologs from fission yeast and human. *Science*, *277*(5328), 955–959. https://doi.org/10.1126/science.277.5328.955

Nawrocki, E. P., & Eddy, S. R. (2013). Infernal 1.1: 100-fold faster RNA homology searches. *Bioinformatics*, *29*(22), 2933–2935. https://doi.org/10.1093/bioinformatics/btt509

Neuner, E., Frener, M., Lusser, A., & Micura, R. (2018). Superior cellular activities of azido- over amino-functionalized ligands for engineered $PreQ_1$ riboswitches in *E. coli*. *RNA Biology*, *15*(10), 1376–1383. https://doi.org/10.1080/15476286.2018.1534526

Nguyen, T. H. D., Tam, J., Wu, R. A., Greber, B. J., Toso, D., Nogales, E., & Collins, K. (2018). Cryo-EM structure of substrate-bound human telomerase holoenzyme. *Nature*, *557*(7704), 190–195. https://doi.org/10.1038/s41586-018-0062-x

Nissen, P., Ippolito, J. A., Ban, N., Moore, P. B., & Steitz, T. A. (2001). RNA tertiary interactions in the large ribosomal subunit: The A-minor motif. *Proceedings of the National Academy of Sciences of the United States of America*, *98*(9), 4899–4903. https://doi.org/10.1073/pnas.081082398081082398

Nissim, L., Perli, S. D., Fridkin, A., Perez-Pinera, P., & Lu, T. K. (2014). Multiplexed and programmable regulation of gene networks with an integrated RNA and CRISPR/Cas toolkit in human cells. *Molecular Cell*, *54*(4), 698–710. https://doi.org/10.1016/j.molcel.2014.04.022

O'Leary, V. B., Ovsepian, S. V., Carrascosa, L. G., Buske, F. A., Radulovic, V., Niyazi, M., ... Anastasov, N. (2015). PARTICLE, a triplex-forming long ncRNA, regulates locus-specific methylation in response to low-dose irradiation. *Cell Reports*, *11*(3), 474–485. https://doi.org/10.1016/j.celrep.2015.03.043

Pendleton, K. E., Chen, B., Liu, K., Hunter, O. V., Xie, Y., Tu, B. P., & Conrad, N. K. (2017). The U6 snRNA m^6A methyltransferase METTL16 regulates SAM synthetase intron retention. *Cell*, *169*(5), 824–835.e814. https://doi.org/10.1016/j.cell.2017.05.003

Peselis, A., & Serganov, A. (2014). Structure and function of pseudoknots involved in gene expression control. *WIREs RNA*, *5*(6), 803–822. https://doi.org/10.1002/wrna.1247

Pham, V. V., Salguero, C., Khan, S. N., Meagher, J. L., Brown, W. C., Humbert, N., ... D'Souza, V. M. (2018). HIV-1 Tat interactions with cellular 7SK and viral TAR RNAs identifies dual structural mimicry. *Nature Communications*, *9*(1), 4266. https://doi.org/10.1038/s41467-018-06591-6

Pilch, D. S., Kirolos, M. A., & Breslauer, K. J. (1995). Berenil binding to higher ordered nucleic acid structures: Complexation with a DNA and RNA triple helix. *Biochemistry*, *34*(49), 16107–16124. https://doi.org/10.1021/bi00049a026

Plum, G. E., & Breslauer, K. J. (1995). Thermodynamics of an intramolecular DNA triple helix: A calorimetric and spectroscopic study of the pH and salt dependence of thermally induced structural transitions. *Journal of Molecular Biology*, *248*(3), 679–695.

Poiata, E., Meyer, M. M., Ames, T. D., & Breaker, R. R. (2009). A variant riboswitch aptamer class for *S*-adenosylmethionine common in marine bacteria. *RNA*, *15*(11), 2046–2056. https://doi.org/10.1261/rna.1824209

Pradhan, A. B., Bhuiya, S., Haque, L., & Das, S. (2018). Role of hydroxyl groups in the B-ring of flavonoids in stabilization of the Hoogsteen paired third strand of poly(U)•poly(A)-poly(U) triplex. *Archives of Biochemistry and Biophysics*, *637*, 9–20. https://doi.org/10.1016/j.abb.2017.11.008

Qiao, F., & Cech, T. R. (2008). Triple-helix structure in telomerase RNA contributes to catalysis. *Nature Structural & Molecular Biology*, *15*(6), 634–640. https://doi.org/10.1038/nsmb.1420

Qu, G., Kaushal, P. S., Wang, J., Shigematsu, H., Piazza, C. L., Agrawal, R. K., ... Wang, H. W. (2016). Structure of a group II intron in complex with its reverse transcriptase. *Nature Structural & Molecular Biology*, *23*(6), 549–557. https://doi.org/10.1038/nsmb.3220

Raghunathan, G., Miles, H. T., & Sasisekharan, V. (1995). Symmetry and structure of RNA and DNA triple helices. *Biopolymers*, *36*(3), 333–343. https://doi.org/10.1002/bip.360360308

Rainen, L. C., & Stollar, B. D. (1977). Antisera to poly(A)-poly(U)-poly(I) contain antibody subpopulations specific for different aspects of the triple helix. *Biochemistry*, *16*(9), 2003–2007. https://doi.org/10.1021/bi00628a038

Ren, J., & Chaires, J. B. (1999). Sequence and structural selectivity of nucleic acid binding ligands. *Biochemistry*, *38*(49), 16067–16075. https://doi.org/10.1021/bi992070s

Ren, J., Rastegari, B., Condon, A., & Hoos, H. H. (2005). HotKnots: Heuristic prediction of RNA secondary structures including pseudoknots. *RNA*, *11*(10), 1494–1504. https://doi.org/10.1261/rna.7284905

Rich, A., & Watson, J. D. (1954). Physical studies on ribonucleic acid. *Nature*, *173*(4412), 995–996. https://doi.org/10.1038/173995a0

Rich, A., & Davies, D. R. (1956). A new two-stranded helical structure: Polyadenylic acid and polyuridylic acid. *Journal of the American Chemical Society*, *78*, 3548–3549.

Rivas, E., & Eddy, S. R. (1999). A dynamic programming algorithm for RNA structure prediction including pseudoknots. *Journal of Molecular Biology*, *285*(5), 2053–2068. https://doi.org/10.1006/jmbi.1998.2436

Robart, A. R., Chan, R. T., Peters, J. K., Rajashankar, K. R., & Toor, N. (2014). Crystal structure of a eukaryotic group II intron lariat. *Nature*, *514*(7521), 193–197. https://doi.org/10.1038/nature13790

Roberts, R. W., & Crothers, D. M. (1996). Prediction of the stability of DNA triplexes. *Proceedings of the National Academy of Sciences of the United States of America*, *93*(9), 4320–4325.

Roy, S., Lammert, H., Hayes, R. L., Chen, B., LeBlanc, R., Dayie, T. K., ... Sanbonmatsu, K. Y. (2017). A magnesium-induced triplex preorganizes the SAM-II riboswitch. *PLoS Computational Biology*, *13*(3), e1005406. https://doi.org/10.1371/journal.pcbi.1005406

Rusling, D. A., Powers, V. E., Ranasinghe, R. T., Wang, Y., Osborne, S. D., Brown, T., & Fox, K. R. (2005). Four base recognition by triplex-forming oligonucleotides at physiological pH. *Nucleic Acids Research*, *33*(9), 3025–3032. https://doi.org/10.1093/nar/gki625

Russo, M., De Lucca, B., Flati, T., Gioiosa, S., Chillemi, G., & Capranico, G. (2019). DROPA: DRIP-seq optimized peak annotator. *BMC Bioinformatics*, *20*(1), 414. https://doi.org/10.1186/s12859-019-3009-9

Ruszkowska, A., Ruszkowski, M., Hulewicz, J. P., Dauter, Z., & Brown, J. A. (2020). Molecular structure of a U•A-U-rich RNA triple helix with 11 consecutive base triples. *Nucleic Acids Research*, *48*(6), 3304–3314. https://doi.org/10.1093/nar/gkz1222

Schindelin, H., Zhang, M., Bald, R., Furste, J. P., Erdmann, V. A., & Heinemann, U. (1995). Crystal structure of an RNA dodecamer containing the *Escherichia coli* Shine-Dalgarno sequence. *Journal of Molecular Biology*, *249*(3), 595–603. https://doi.org/10.1006/jmbi.1995.0321

Semerad, C. L., & Maher, L. J., 3rd. (1994). Exclusion of RNA strands from a purine motif triple helix. *Nucleic Acids Research*, *22*(24), 5321–5325. https://doi.org/10.1093/nar/22.24.5321

Senturk Cetin, N., Kuo, C. C., Ribarska, T., Li, R., Costa, I. G., & Grummt, I. (2019). Isolation and genome-wide characterization of cellular DNA:RNA triplex structures. *Nucleic Acids Research*, *47*(5), 2306–2321. https://doi.org/10.1093/nar/gky1305

Sharma, E., Sterne-Weiler, T., O'Hanlon, D., & Blencowe, B. J. (2016). Global mapping of human RNA-RNA interactions. *Molecular Cell*, *62*(4), 618–626. https://doi.org/10.1016/j.molcel.2016.04.030

Shay, J. W. (2016). Role of telomeres and telomerase in aging and cancer. *Cancer Discovery*, *6*(6), 584–593. https://doi.org/10.1158/2159-8290.CD-16-0062

Shay, J. W., & Bacchetti, S. (1997). A survey of telomerase activity in human cancer. *European Journal of Cancer*, *33*(5), 787–791. https://doi.org/10.1016/S0959-8049(97)00062-2

Shefer, K., Brown, Y., Gorkovoy, V., Nussbaum, T., Ulyanov, N. B., & Tzfati, Y. (2007). A triple helix within a pseudoknot is a conserved and essential element of telomerase RNA. *Molecular and Cellular Biology*, *27*(6), 2130–2143. https://doi.org/10.1128/MCB.01826-06

Sherlock, M. E., & Breaker, R. R. (2017). Biochemical validation of a third guanidine riboswitch class in bacteria. *Biochemistry*, *56*(2), 359–363. https://doi.org/10.1021/acs.biochem.6b01271

Singleton, S. F., & Dervan, P. B. (1992). Influence of pH on the equilibrium association constants for oligodeoxyribonucleotide-directed triple helix formation at single DNA sites. *Biochemistry*, *31*(45), 10995–11003. https://doi.org/10.1021/bi00160a008

Sinha, R., & Kumar, G. S. (2009). Interaction of isoquinoline alkaloids with an RNA triplex: Structural and thermodynamic studies of berberine, palmatine, and coralyne binding to poly(U)•poly(A)-poly(U). *Journal of Physical Chemistry. B*, *113*(40), 13410–13420. https://doi.org/10.1021/jp9069515

Smathers, C. M., & Robart, A. R. (2019). The mechanism of splicing as told by group II introns: Ancestors of the spliceosome. *Biochimica et Biophysica Acta, Gene Regulatory Mechanisms*, *1862*(11–12), 194390. https://doi.org/10.1016/j.bbagrm.2019.06.001

Smith, K. D., Shanahan, C. A., Moore, E. L., Simon, A. C., & Strobel, S. A. (2011). Structural basis of differential ligand recognition by two classes of bis-(3′-5′)-cyclic dimeric guanosine monophosphate-binding riboswitches. *Proceedings of the National Academy of Sciences of the United States of America*, *108*(19), 7757–7762. https://doi.org/10.1073/pnas.1018857108

Sontheimer, E. J., Gordon, P. M., & Piccirilli, J. A. (1999). Metal ion catalysis during group II intron self-splicing: Parallels with the spliceosome. *Genes & Development*, *13*(13), 1729–1741. https://doi.org/10.1101/gad.13.13.1729

Sontheimer, E. J., Sun, S., & Piccirilli, J. A. (1997). Metal ion catalysis during splicing of premessenger RNA. *Nature*, *388*(6644), 801–805. https://doi.org/10.1038/42068

Souliere, M. F., Altman, R. B., Schwarz, V., Haller, A., Blanchard, S. C., & Micura, R. (2013). Tuning a riboswitch response through structural extension of a pseudoknot. *Proceedings of the National Academy of Sciences of the United States of America*, *110*(35), E3256–E3264. https://doi.org/10.1073/pnas.1304585110

Steitz, T. A., & Steitz, J. A. (1993). A general two-metal-ion mechanism for catalytic RNA. *Proceedings of the National Academy of Sciences of the United States of America*, *90*(14), 6498–6502. https://doi.org/10.1073/pnas.90.14.6498

Stollar, B. D., & Raso, V. (1974). Antibodies recognise specific structures of triple-helical polynucleotides built on poly(A) or poly(dA). *Nature*, *250*(463), 231–234.

Su, L., Chen, L., Egli, M., Berger, J. M., & Rich, A. (1999). Minor groove RNA triplex in the crystal structure of a ribosomal frameshifting viral pseudoknot. *Nature Structural Biology*, *6*(3), 285–292. https://doi.org/10.1038/6722

Sun, R., Lin, S. F., Gradoville, L., & Miller, G. (1996). Polyadenylylated nuclear RNA encoded by Kaposi sarcoma-associated herpesvirus. *Proceedings of the National Academy of Sciences of the United States of America*, *93*(21), 11883–11888.

Sunwoo, H., Dinger, M. E., Wilusz, J. E., Amaral, P. P., Mattick, J. S., & Spector, D. L. (2009). MENε/β nuclear-retained non-coding RNAs are upregulated upon muscle differentiation and are essential components of paraspeckles. *Genome Research*, *19*(3), 347–359. https://doi.org/10.1101/gr.087775.108

Sussman, J. L., Holbrook, S. R., Warrant, R. W., Church, G. M., & Kim, S. H. (1978). Crystal structure of yeast phenylalanine transfer RNA. I. Crystallographic Refinement. *Journal of Molecular Biology*, *123*(4), 607–630. https://doi.org/10.1016/0022-2836(78)90209-7

Szewczak, A. A., Ortoleva-Donnelly, L., Ryder, S. P., Moncoeur, E., & Strobel, S. A. (1998). A minor groove RNA triple helix within the catalytic core of a group I intron. *Nature Structural Biology*, *5*(12), 1037–1042. https://doi.org/10.1038/4146

Tabaska, J. E., Cary, R. B., Gabow, H. N., & Stormo, G. D. (1998). An RNA folding method capable of identifying pseudoknots and base triples. *Bioinformatics*, *14*(8), 691–699. https://doi.org/10.1093/bioinformatics/14.8.691

Tanaka, Y., Fujii, S., Hiroaki, H., Sakata, T., Tanaka, T., Uesugi, S., … Kyogoku, Y. (1999). A′-form RNA double helix in the single crystal structure of r(UGAGCUUCGGCUC). *Nucleic Acids Research*, *27*(4), 949–955. https://doi.org/10.1093/nar/27.4.949

Theimer, C. A., Blois, C. A., & Feigon, J. (2005). Structure of the human telomerase RNA pseudoknot reveals conserved tertiary interactions essential for function. *Molecular Cell*, *17*(5), 671–682. https://doi.org/10.1016/j.molcel.2005.01.017

Thomas, T. J., Seibold, J. R., Adams, L. E., & Hess, E. V. (1995). Triplex-DNA stabilization by hydralazine and the presence of anti-(triplex DNA) antibodies in patients treated with hydralazine. *Biochemical Journal*, *311*(Pt 1), 183–188. https://doi.org/10.1042/bj3110183

Tiwari, R., Haque, L., Bhuiya, S., & Das, S. (2017). Third strand stabilization of poly(U)•poly(A)-poly(U) triplex by the naturally occurring flavone luteolin: A multi-spectroscopic approach. *International Journal of Biological Macromolecules*, *103*, 692–700. https://doi.org/10.1016/j.ijbiomac.2017.05.115

Toor, N., Keating, K. S., Taylor, S. D., & Pyle, A. M. (2008). Crystal structure of a self-spliced group II intron. *Science*, *320*(5872), 77–82. https://doi.org/10.1126/science.1153803

Tseng, C. K., Wang, H. F., Schroeder, M. R., & Baumann, P. (2018). The H/ACA complex disrupts triplex in hTR precursor to permit processing by RRP6 and PARN. *Nature Communications*, *9*(1), 5430. https://doi.org/10.1038/s41467-018-07822-6

Tycowski, K. T., Shu, M. D., Borah, S., Shi, M., & Steitz, J. A. (2012). Conservation of a triple-helix-forming RNA stability element in noncoding and genomic RNAs of diverse viruses. *Cell Reports*, *2*(1), 26–32. https://doi.org/10.1016/j.celrep.2012.05.020

Tycowski, K. T., Shu, M. D., & Steitz, J. A. (2016). Myriad triple-helix-forming structures in the transposable element RNAs of plants and fungi. *Cell Reports*, *15*(6), 1266–1276. https://doi.org/10.1016/j.celrep.2016.04.010

Tzfati, Y., Knight, Z., Roy, J., & Blackburn, E. H. (2003). A novel pseudoknot element is essential for the action of a yeast telomerase. *Genes & Development*, *17*(14), 1779–1788. https://doi.org/10.1101/gad.1099403

Ulyanov, N. B., Shefer, K., James, T. L., & Tzfati, Y. (2007). Pseudoknot structures with conserved base triples in telomerase RNAs of ciliates. *Nucleic Acids Research*, *35*(18), 6150–6160. https://doi.org/10.1093/nar/gkm660

van Vlack, E. R., Topp, S., & Seeliger, J. C. (2017). Characterization of engineered $PreQ_1$ riboswitches for inducible gene regulation in mycobacteria. *Journal of Bacteriology*, *199*(6), e00656-16. https://doi.org/10.1128/JB.00656-16

Varani, G., & McClain, W. H. (2000). The G•U wobble base pair. A fundamental building block of RNA structure crucial to RNA function in diverse biological systems. *EMBO Reports*, *1*(1), 18–23. https://doi.org/10.1093/embo-reports/kvd001

Vogan, J. M., Zhang, X., Youmans, D. T., Regalado, S. G., Johnson, J. Z., Hockemeyer, D., & Collins, K. (2016). Minimized human telomerase maintains telomeres and resolves endogenous roles of H/ACA proteins, TCAB1, and Cajal bodies. *Elife*, *5*, e18221. https://doi.org/10.7554/eLife.18221

Volker, J., & Klump, H. H. (1994). Electrostatic effects in DNA triple helices. *Biochemistry*, *33*(45), 13502–13508.

Wan, R., Yan, C., Bai, R., Huang, G., & Shi, Y. (2016). Structure of a yeast catalytic step I spliceosome at 3.4-Å resolution. *Science*, *353*(6302), 895–904. https://doi.org/10.1126/science.aag2235

Wang, S., Friedman, A. E., & Kool, E. T. (1995). Origins of high sequence selectivity: A stopped-flow kinetics study of DNA/RNA hybridization by duplex- and triplex-forming oligonucleotides. *Biochemistry*, *34*(30), 9774–9784. https://doi.org/10.1021/bi00030a015

Wang, T., Chen, C., Larcher, L. M., Barrero, R. A., & Veedu, R. N. (2019). Three decades of nucleic acid aptamer technologies: Lessons learned, progress and opportunities on aptamer development. *Biotechnology Advances*, *37*(1), 28–50. https://doi.org/10.1016/j.biotechadv.2018.11.001

Warda, A. S., Kretschmer, J., Hackert, P., Lenz, C., Urlaub, H., Hobartner, C., … Bohnsack, M. T. (2017). Human METTL16 is a N^6-methyladenosine (m^6A) methyltransferase that targets pre-mRNAs and various non-coding RNAs. *EMBO Reports*, *18*(11), 2004–2014. https://doi.org/10.15252/embr.201744940

Warnasooriya, C., Ling, C., Belashov, I. A., Salim, M., Wedekind, J. E., & Ermolenko, D. N. (2019). Observation of $PreQ_1$-II riboswitch dynamics using single-molecule FRET. *RNA Biology*, *16*(9), 1086–1092. https://doi.org/10.1080/15476286.2018.1536591

Watson, J. D., & Crick, F. H. (1953). The structure of DNA. *Cold Spring Harbor Symposia on Quantitative Biology*, *18*, 123–131.

Wilkinson, M. E., Charenton, C., & Nagai, K. (2019). RNA splicing by the spliceosome. *Annual Review of Biochemistry*, *89*, 1.1–1.30. https://doi.org/10.1146/annurev-biochem-091719-064225

Wilusz, J. E., Freier, S. M., & Spector, D. L. (2008). 3′-end processing of a long nuclear-retained noncoding RNA yields a tRNA-like cytoplasmic RNA. *Cell*, *135*(5), 919–932. https://doi.org/10.1016/j.cell.2008.10.012

Wilusz, J. E., JnBaptiste, C. K., Lu, L. Y., Kuhn, C. D., Joshua-Tor, L., & Sharp, P. A. (2012). A triple helix stabilizes the 3′ ends of long noncoding RNAs that lack poly(A) tails. *Genes & Development*, *26*(21), 2392–2407. https://doi.org/10.1101/gad.204438.112gad.204438.112

Wu, R. A., Upton, H. E., Vogan, J. M., & Collins, K. (2017). Telomerase mechanism of telomere synthesis. *Annual Review of Biochemistry*, *86*, 439–460. https://doi.org/10.1146/annurev-biochem-061516-045019

Xodo, L. E., Manzini, G., Quadrifoglio, F., van der Marel, G. A., & van Boom, J. H. (1991). Effect of 5-methylcytosine on the stability of triple-stranded DNA—A thermodynamic study. *Nucleic Acids Research*, *19*(20), 5625–5631. https://doi.org/10.1093/nar/19.20.5625

Yamada, M., Watanabe, Y., Gootenberg, J. S., Hirano, H., Ran, F. A., Nakane, T., ... Nureki, O. (2017). Crystal structure of the minimal Cas9 from *Campylobacter jejuni* reveals the molecular diversity in the CRISPR-Cas9 systems. *Molecular Cell*, *65*(6), 1109–1121.e1103. https://doi.org/10.1016/j.molcel.2017.02.007

Yan, C., Hang, J., Wan, R., Huang, M., Wong, C. C., & Shi, Y. (2015). Structure of a yeast spliceosome at 3.6-Å resolution. *Science*, *349*(6253), 1182–1191. https://doi.org/10.1126/science.aac7629

Yan, C., Wan, R., Bai, R., Huang, G., & Shi, Y. (2016). Structure of a yeast activated spliceosome at 3.5-Å resolution. *Science*, *353*(6302), 904–911. https://doi.org/10.1126/science.aag0291

Yang, S. Y., Lejault, P., Chevrier, S., Boidot, R., Robertson, A. G., Wong, J. M. Y., & Monchaud, D. (2018). Transcriptome-wide identification of transient RNA G-quadruplexes in human cells. *Nature Communications*, *9*(1), 4730. https://doi.org/10.1038/s41467-018-07224-8

Yean, S. L., Wuenschell, G., Termini, J., & Lin, R. J. (2000). Metal-ion coordination by U6 small nuclear RNA contributes to catalysis in the spliceosome. *Nature*, *408*(6814), 881–884. https://doi.org/10.1038/35048617

Yonkunas, M. J., & Baird, N. J. (2019). A highly ordered, nonprotective MALAT1 ENE structure is adopted prior to triplex formation. *RNA*, *25*(8), 975–984. https://doi.org/10.1261/rna.069906.118

Zhan, H., Xie, H., Zhou, Q., Liu, Y., & Huang, W. (2018). Synthesizing a genetic sensor based on CRISPR-Cas9 for specifically killing p53-deficient cancer cells. *ACS Synthetic Biology*, *7*(7), 1798–1807. https://doi.org/10.1021/acssynbio.8b00202

Zhang, B., Mao, Y. S., Diermeier, S. D., Novikova, I. V., Nawrocki, E. P., Jones, T. A., ... Spector, D. L. (2017). Identification and characterization of a class of MALAT1-like genomic loci. *Cell Reports*, *19*(8), 1723–1738. https://doi.org/10.1016/j.celrep.2017.05.006

Zhang, L., Vielle, A., Espinosa, S., & Zhao, R. (2019). RNAs in the spliceosome: Insight from cryo-EM structures. *WIREs RNA*, *10*(3), e1523. https://doi.org/10.1002/wrna.1523

Zhao, Z., Senturk, N., Song, C., & Grummt, I. (2018). lncRNA PAPAS tethered to the rDNA enhancer recruits hypophosphorylated CHD4/NuRD to repress rRNA synthesis at elevated temperatures. *Genes & Development*, *32*(11–12), 836–848. https://doi.org/10.1101/gad.311688.118

Zhong, W., Wang, H., Herndier, B., & Ganem, D. (1996). Restricted expression of Kaposi sarcoma-associated herpesvirus (human herpesvirus 8) genes in Kaposi sarcoma. *Proceedings of the National Academy of Sciences of the United States of America*, *93*(13), 6641–6646.

Zuidema, D., Van den Berg, F. M., & Flavell, R. A. (1978). The isolation of duplex DNA fragments containing (dG-dC) clusters by chromatography on poly(rC)-Sephadex. *Nucleic Acids Research*, *5*(7), 2471–2483. https://doi.org/10.1093/nar/5.7.2471

How to cite this article: Brown JA. Unraveling the structure and biological functions of RNA triple helices. *WIREs RNA*. 2020;11:e1598. https://doi.org/10.1002/wrna.1598